2019

Detection of TAR DNA-binding protein 43 (TDP-43) oligomers as initial intermediate species during aggregate formation

Rachel L. French

Zachary R. Grese

Himani Aligireddy

Dhruva D. Dhavale

Ashley N. Reeb

See next page for additional authors

Authors

Rachel L. French, Zachary R. Grese, Himani Aligireddy, Dhruva D. Dhavale, Ashley N. Reeb, Niraja Kedia, Paul T. Kotzbauer, Jan Bieschke, and Yuna M. Ayala

Detection of TAR DNA-binding protein 43 (TDP-43) oligomers as initial intermediate species during aggregate formation

Received for publication, September 18, 2018, and in revised form, February 27, 2019 Published, Papers in Press, March 1, 2019, DOI 10.1074/jbc.RA118.005889

Rachel L. French[‡], Zachary R. Grese[‡], Himani Aligireddy[‡], Dhruva D. Dhavale[§], Ashley N. Reeb[‡1], Niraja Kedia[¶], Paul T. Kotzbauer[§], Jan Bieschke[¶], and Yuna M. Ayala[‡2]

From the [‡]Edward A. Doisy Department of Biochemistry and Molecular Biology, Saint Louis University, St. Louis, Missouri 63103, the [§]Department of Neurology, Washington University School of Medicine, St. Louis, Missouri 63110, and the [¶]MRC Prion Unit, University College London, London W1W 7FF, United Kingdom

Edited by Paul E. Fraser

Aggregates of the RNA-binding protein TDP-43 (TAR DNA-binding protein) are a hallmark of the overlapping neurodegenerative disorders amyotrophic lateral sclerosis (ALS) and frontotemporal dementia. The process of TDP-43 aggregation remains poorly understood, and whether it includes formation of intermediate complexes is unknown. Here, we analyzed aggregates derived from purified TDP-43 under semidenaturing conditions, identifying distinct oligomeric complexes at the initial time points before the formation of large aggregates. We found that this early oligomerization stage is primarily driven by TDP-43's RNA-binding region. Specific binding to GU-rich RNA strongly inhibited both TDP-43 oligomerization and aggregation, suggesting that RNA interactions are critical for maintaining TDP-43 solubility. Moreover, we analyzed TDP-43 liquid–liquid phase separation and detected similar detergent-resistant oligomers upon maturation of liquid droplets into solid-like fibrils. These results strongly suggest that the oligomers form during the early steps of TDP-43 misfolding. Importantly, the ALS-linked TDP-43 mutations A315T and M337V significantly accelerate aggregation, rapidly decreasing the monomeric population and shortening the oligomeric phase. We also show that aggregates generated from purified TDP-43 seed intracellular aggregation detected by established TDP-43 pathology markers. Remarkably, cytoplasmic aggregate seeding was detected earlier for the A315T and M337V variants and was 50% more widespread than for WT TDP-43 aggregates. We provide evidence for an initial step of TDP-43 self-assembly into intermediate oligomeric complexes, whereby these complexes may provide a scaffold for aggregation. This process is altered by ALS-linked mutations, underscoring the role of perturbations in TDP-43 homeostasis in protein aggregation and ALS-FTD pathogenesis.

TDP-43 pathology is a hallmark of amyotrophic lateral sclerosis (ALS)[3] and frontotemporal dementia (FTD). TDP-43 aggregates accumulate in ~98% of ALS and 50% of FTD cases, also defined as ubiquitin-positive frontotemporal lobar degeneration (FTLD-U or FTLD-TDP) (1, 2). In addition, TDP-43 pathology is found in ~50% of Alzheimer's disease (3, 4). The direct role of TDP-43 in disease is underscored by greater than 40 ALS-associated dominant missense mutations in the TDP-43 gene (*TARDBP*) (5). These cause ~3–5 and 1% of familial and sporadic ALS, respectively. The clinicopathological characteristics of ALS and FTD associated with mutant and WT *TARDBP* are largely indistinguishable, and the mechanisms affected by the mutations linked to pathogenesis have not been clearly established. Whether disease results from gain of toxic properties through aggregation, from sequestration of functional TDP-43 into aggregates (1), or from a combination of both, it is increasingly evident that loss of TDP-43 homeostasis and aggregation play a critical role in pathogenesis.

TDP-43 is a highly conserved RNA-binding protein and, like other heterogeneous nuclear ribonucleoproteins (hnRNPs), is composed of modular domains that mediate single-stranded RNA/DNA binding and protein interactions (6–8). Of the two canonical RNA recognition motifs (RRMs), RRM1 contributes to the high affinity for RNA/DNA and GU-rich RNA specificity (6, 7). RRM2 is also highly evolutionarily conserved; however, its function remains unclear. An additional folded domain is at the N terminus, which mediates self-assembly as an isolated domain and presumably of the full-length protein (9–11). The C-terminal domain (CTD) is intrinsically disordered and is a typical low sequence complexity domain, which is highly represented in RNA-binding proteins (12, 13). This domain mediates self-assembly and interactions with hnRNP complexes important for RNA processing activity (8, 14, 15), but at the same time, the CTD drives protein aggregation and toxicity (16–18). The CTD is characterized by an abundance of glutamine/asparagine residues, showing great similarity to prion

This work was supported by the President's Research Fund of Saint Louis University Grant 230230, by Amyotrophic Lateral Sclerosis Association and ALS Finding a Cure, and by NINDS, National Institutes of Health Grant K01 NS082391. This work study was also supported in part by Alzheimer's Disease Core Center Grant P30AG013854 from NIA, National Institutes of Health to Northwestern University (Chicago, IL). The authors declare that they have no conflicts of interest with the contents of this article. The content is solely the responsibility of the authors and does not necessarily represent the official views of the National Institutes of Health.

This article contains Table S1 and Figs. S1–S5.

[1] Present address: Dept. of Otolaryngology, Head and Neck Surgery, Washington University School of Medicine, St. Louis, Missouri 63110.

[2] To whom correspondence should be addressed. Tel.: 314-977-9247; E-mail: yuna.ayala@health.slu.edu.

[3] The abbreviations used are: ALS, amyotrophic lateral sclerosis; FTD, frontotemporal dementia; hnRNP, heterogeneous nuclear ribonucleoprotein; RRM, RNA recognition motif; CTD, C-terminal domain; SDD-AGE, semidenaturing detergent-agarose electrophoresis; β-ME, β-mercaptoethanol; ThioT, thioflavin T; ThioS, thioflavin S; TCEP, Tris(2-carboxyethyl)phosphine; LLPS, liquid–liquid phase separation; RIPA. radioimmune precipitation assay; AFM, atomic force microscopy; NLS, nuclear localization signal; PI, protease inhibitor; DAPI, 4′,6′-diamino-2-phenylindole.

domains in yeast proteins, such as that of the archetypal prion protein Sup35 (13, 19). Significantly, almost all disease-associated TDP-43 mutations cluster in the CTD (5, 20), strongly suggesting that these substitutions disrupt normal protein interactions and promote aggregate formation, driving the disease state.

The central mechanism in TDP-43 self-assembly and aggregation has been largely unexplored. TDP-43 aggregation assays using the full-length protein are encumbered by the extreme aggregation-prone characteristic of TDP-43, which makes production of pure soluble protein particularly challenging. Having recently established methods to generate soluble recombinant TDP-43 (21), we studied its aggregation to identify the factors that mediate and alter this process (*e.g.* ALS-associated mutations) and to gain insight into the structure of aggregates. We found that TDP-43 aggregates are formed through a biphasic process that initiates with oligomerization followed by aggregation into high-molecular-weight polymers. ALS-linked mutants potently affect aggregation by increasing the rate of assembly. In addition, we show that the aggregates derived from purified TDP-43 are capable of seeding intracellular aggregation following uptake. Our results support a model in which TDP-43 undergoes self-assembly into oligomeric complexes upon misfolding that act as templates for large aggregates. This process may be altered in disease conditions, such as in the presence of patient-linked mutations.

Results

TDP-43 oligomers assemble at the initial aggregation stage followed by high molecular weight aggregates

We have successfully developed methods to generate full-length bacterial recombinant TDP-43 (rTDP-43) to characterize TDP-43 interactions (21) (Fig. S1*A*). We expressed and purified homogeneous and soluble TDP-43 N-terminally fused to SUMO (21), which is cleaved off by the SUMO deconjugating protease Ulp1 (Fig. S1*B*). Using this protein, we analyzed TDP-43 self-assembly and aggregation. Prior to carrying out the aggregation assays, we ensured that purified protein preparations did not include preformed aggregates using high-speed ultracentrifugation and by routinely measuring protein activity in RNA-binding assays (Fig. S1*C*). The binding affinity for the TDP-43–$A(GU)_6$ RNA interaction was determined with our previously established fluorescence-based method (21). This accurately measures the apparent dissociation constant for $A(GU)_6$ (typically $K_{d,\,app} = 2.3 \pm 0.7$ nM) and also provides an estimate of the active protein concentration. By measuring these parameters and assuming that active protein concentration is equal to the concentration of soluble protein, we determined the purity of our protein preparations. Our aggregation assays consisted of analyzing rTDP-43 complexes after brief shaking followed by incubation at room temperature (~22 °C). To detect the assembled complexes, we adapted a method widely used for the characterization of yeast prion aggregates (22–24), based on the resolution of soluble and large aggregate complexes by semidenaturing detergent-agarose electrophoresis (SDD-AGE). SDD-AGE generates large pores allowing the detection of large protein complexes that are resistant to SDS detergent, typically ranging from 0.1 to 2% (24). This method has also been used to detect neurodegeneration-associated aggregates, such as Tau (25), and in a limited number of studies to analyze TDP-43 pathology from patient tissue and cultured cells (26, 27). We analyzed rTDP-43 aggregates formed over time and obtained the resolution of rTDP-43 monomers and large polymers, which increased in size (Fig. 1*A*). In addition to the expected high-molecular-weight aggregates, we observed an oligomeric pattern of assembly at initial time points. These initial complexes (Figs. 1*A*, days 1–4, *arrows*) were replaced by larger, heterogeneous species at longer incubation times (Fig. 1*A*, days 8–15). The later-day large complexes resembled aggregates formed by prion proteins and other protein aggregates analyzed with this method (22, 25, 28). Addition of polyethylene glycol, used as a crowding agent, accelerated the aggregation rate, increasing the formation of the larger complexes (Fig. S2*A*). Fig. 1 shows complexes formed by SUMO-tagged TDP-43, and removal of SUMO had no significant effect in the size of the aggregates or in the formation of oligomers (Fig. S2*B*). In the absence of SUMO, the assays were initiated immediately after removal of the tag because the cleaved

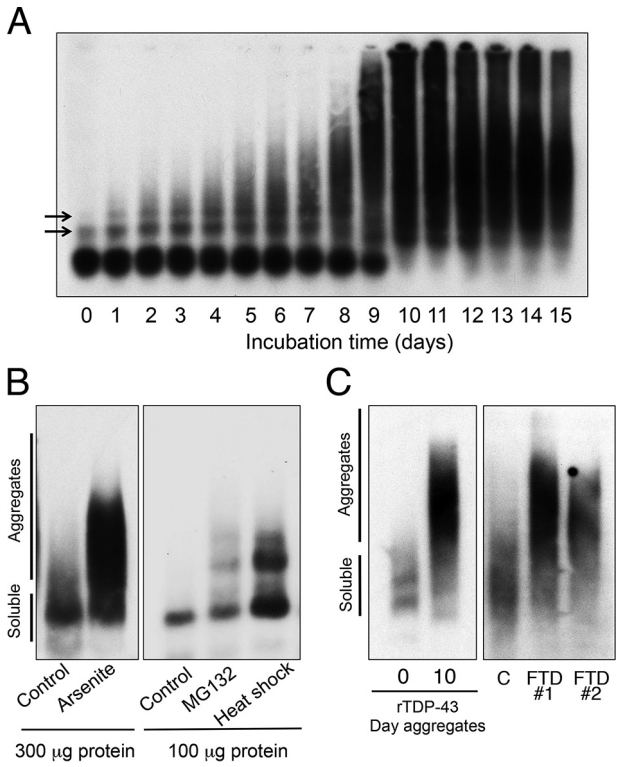

Figure 1. Detection of TDP-43 oligomers during the initial steps of aggregation. SDD-AGE and immunoblotting analysis to detect TDP-43 aggregates using purified protein, cells treated with proteotoxic stress, and FTD patient samples. *A*, aggregation of full-length purified TDP-43 (rTDP-43) was triggered by brief shaking (2 μM in reaction buffer), and samples were analyzed as a function of time. Day 0 was collected immediately after triggering aggregation by shaking. *Arrows* point to the initial oligomeric species. *B*, lysates from HEK293 cells treated with sodium arsenite, the ubiquitin proteasome system inhibitor MG132 (10 μM, 4 h), heat shock (43 °C for 30 min), and nontreated control. Either 300 or 100 μg of total protein was loaded. *C*, the sarkosyl-insoluble fraction from FTD and control (*lane C*) brain samples analyzed by SDD-AGE. These were compared with day 0 and day 10 rTDP-43 aggregates prepared in the same buffer conditions as the brain samples. All blots were probed with TDP-43 antibody and are representative of more than three individual experiments.

TDP-43 could not be stored without significant protein loss. Therefore, we used SUMO-tagged protein in our experiments, unless noted.

We compared aggregates from purified TDP-43 to cell-derived aggregates and insoluble TDP-43 fractions from FTD brain tissue samples to validate our methods for aggregate characterization and to assess the physiological relevance of the rTDP-43complexes detected using SDD-AGE. Lysates from human embryonic kidney (HEK293) cells under conditions known to promote TDP-43 aggregation, oxidative stress treatment with sodium arsenite (29), showed high-molecular-weight complexes similar to the later-day rTDP-43 aggregates (Fig. 1*B*). They were absent in nontreated control cell lysates. Milder proteotoxic conditions, such as inhibition of the ubiquitin proteasome system with 10 μM MG132 or 30 min of heat shock (21, 30, 31), increased the presence of a distinct high-molecular-weight complex migrating above monomeric TDP-43. The physiological oligomerization of TDP-43 into higher order complexes in cells, ranging in size from monomers to much larger macromolecular assemblies has been previously reported (9, 27). In our analysis, TDP-43 from control-treated lysates migrated as monomers, indicating that these complexes were reversible and destroyed in the presence of detergent. On the other hand, distinct higher order complexes detected by SDD-AGE upon treatment with MG132 and heat shock suggested that misfolding under these conditions promoted strong interactions resistant to semidenaturing agents. Based on these findings, we propose that the early-day oligomers during the initial rTDP-43 aggregation stage are the counterparts of misfolded complexes in cells. These species may be detected under specific conditions, resulting in loss of proteostasis and perhaps even in physiological complexes, such as the recently described TDP-43 myo-granules found in skeletal muscle (32). Next, we analyzed postmortem human brain tissue from control and FTD cases following sequential extraction of gray matter dissected from frontal cortex samples (Fig. 1*C*). We used the sarkosyl insoluble fraction for our analyses as described under "Experimental procedures" (33). Our results showed that the levels of TDP-43 aggregates in FTD samples increased compared with control, consistent with a previous report (26). In addition, the migration pattern of TDP-43 in control tissue was different from the disease cases. We included 0- and 10-day rTDP-43 aggregates in the same solution conditions as brain tissue for comparison (Fig. 1*C*). This showed that migration of later-day rTDP-43 aggregates was similar to TDP-43 complexes from FTD but not from control tissue. Collectively, these results suggest that our methods may be used to detect and analyze aggregate species generated from the purified protein, which show conformational and biochemical similarities to cell and patient-derived TDP-43 inclusions.

We investigated whether TDP-43 complexes could be detected without triggering aggregation by shaking and found that 10 min of incubation of soluble protein at increasing temperatures enhanced the formation of oligomers as seen by SDD-AGE (Fig. 2*A*). The *left panel* of Fig. 2*A* shows aggregates formed at 0, 3, 5, and 10 days after shaking, for comparison. The TDP-43 complexes, which increase at higher temperatures, are similar to the intermediate species in the aggregation assay. To

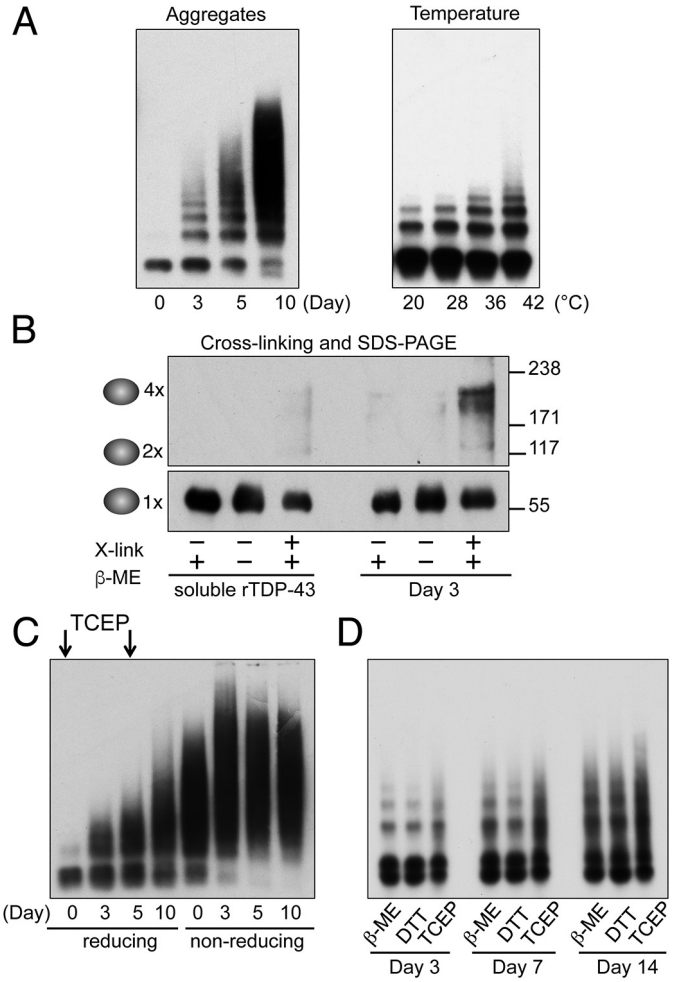

Figure 2. TDP-43 oligomers increase at higher temperatures and are not mediated by covalent disulfide bonds. *A*, SDD-AGE/immunoblotting analysis of aggregates formed at 0, 3, 5, and 10 days compared with TDP-43 complexes formed upon brief incubation at increasing temperatures without shaking (2 μM TDP-43 in reaction buffer at 20–42 °C for 10 min). *B*, days 0 and 3 TDP-43 complexes were chemically cross-linked (*X-link*) in the presence and absence of 250 mM β-ME). Samples were analyzed by SDS-PAGE and immunoblot. The estimated number of TDP-43 molecules cross-linked, and the molecular mass markers (kDa) are shown. *C*, SDD-AGE analysis of rTDP-43 aggregates under reducing conditions, TCEP was added throughout the purification and supplemented at day 5 (reducing). *Arrows* point to the time of addition of extra TCEP. In nonreducing conditions, TDP-43 was purified in the presence of the short-lived reducing agent β-ME, and no additional reducing agents were added during the assay. *D*, day 3, 7, and 14 aggregates prepared in the presence of TCEP and treated with high concentrations of reducing agents (250 mM β-ME, DTT, and TCEP). A longer gel was used to increase oligomer separation. All blots were probed with TDP-43 antibody and are representative of more than three individual experiments.

estimate the oligomeric state of the early TDP-43 complexes, we performed cross-linking experiments under reducing conditions (Fig. 2*B*). These complexes were analyzed by standard denaturing SDS-PAGE after the addition of β-ME (100 mM). As control, non–cross-linked samples were analyzed in the presence and absence of β-ME. Immunoblots showed cross-linked complexes corresponding to tetramers at day 3, according to the estimated molecular weight. This complex was not detected in non–cross-linked samples independent of β-ME treatment. Thus, we propose that initial rTDP-43 self-assembly favors tetrameric complexes formed through interactions not mediated by disulfide bonds.

Thioflavin reactivity with TDP-43 aggregates, including samples derived from patient brain, remains controversial (34–37). The fluorescence of this compound increases upon binding to amyloid structures that accumulate cross-β sheets. We tested binding of rTDP-43 and cellular aggregates to thioflavin T (ThioT) and S (ThioS). ThioT was incubated with rTDP43 monomer for 2 h at room temperature to allow formation of early TDP43 aggregates. We did not observe any significant binding of ThioT to early rTDP43 aggregates under low-salt aggregate-forming conditions. In contrast, the same concentration of α-synuclein fibrils showed a concentration-dependent increase in ThioT fluorescence signal, consistent with previous findings (38) (Fig. S3*A*). Similar results were obtained upon ThioT incubation with 2- and 10-day rTDP-43 aggregates (data not shown). In addition, cellular aggregates, positive for the pSer-409/410 marker of TDP-43 pathology, were not detected by ThioT or ThioS (Fig. S3*B*). These results are in agreement with previous data showing the lack of ThioT binding to rTDP-43, especially when compared with established amyloid aggregates, such as A-β and Sup35 (16, 37). Recently, Vogler *et al.* (32) reported ThioT reactivity with TDP-43 complexes in myogranules from the muscle of a *Vcp* mutant mouse model of multisystem proteinopathy and inclusion body myopathy, which is characterized by TDP-43 aggregation. The discrepancy in the reports from various studies may be caused by differences in TDP-43 complex/aggregate structures formed under the various conditions. Some isoforms may adopt cross-β sheet structure, which may be absent or buried in others. Consistent with this idea, isolated C-terminal peptides show ThioT/S binding upon fibrillization (27, 39–42).

Early TDP-43 complexes are not mediated by disulfide bonds

To further understand whether the TDP-43 complexes detected by SDD-AGE were mediated by covalent interactions, we analyzed their sensitivity to reducing agents. The reducing agent Tris(2-carboxyethyl)phosphine (TCEP) was used throughout rTDP-43 purification and during the aggregation assays. In Fig. 2*C* we added supplementary TCEP on day 5 to ensure that the samples remained under reducing conditions. This was compared with a "nonreducing" assay, whereby aggregates were generated using rTDP-43 purified in the presence of β-ME, a less stable reducing agent compared with TCEP. No additional reducing agent was used in the aggregation assay (nonreducing; Fig. 2*C*). Nonreducing conditions generated large heterogeneous aggregates immediately, beginning at the initial time point (day 0). From these experiments we observed that the initial and intermediate aggregates were detected in the presence of TCEP; however, the larger aggregates decreased significantly under these conditions (*i.e.* day 10 in reducing and nonreducing samples). To further confirm our results, we treated aggregates formed at days 3, 7, and 14 with high concentrations of reducing agents (TCEP, β-ME, and DTT, 250 mM) (Fig. 2*D*). This did not significantly affect the initial complexes but greatly decreased formation of the largest aggregates at later time points. Based on these collective observations we propose that initial complexes that are detected as ordered molecular assemblies by SDD-AGE are partially detergent-resistant oligomers and are not mediated by covalent bonds. On the other hand, the higher-molecular-weight heterogeneous aggregates form through disulfide interactions. This is consistent with the effect of oxidative stress in promoting TDP-43 aggregation in cells and with the previous identification of intra and intermolecular TDP-43 Cys interactions in patient tissue (43). Our results and this previous work highlight the relevance of disulfide bond formation on TDP-43 pathology.

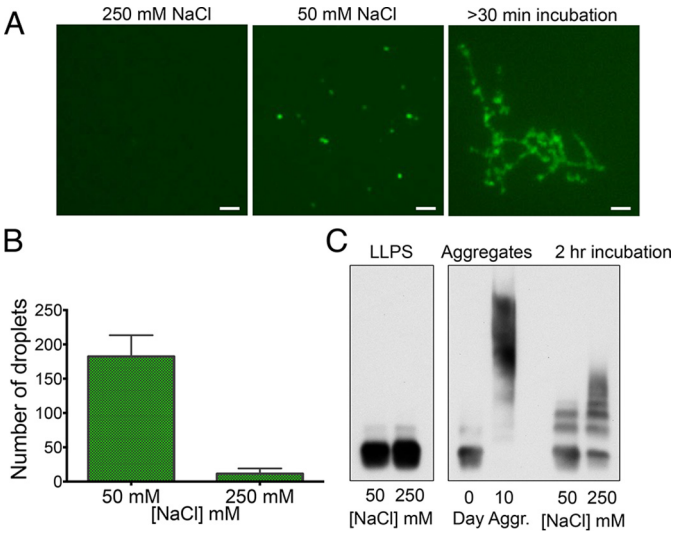

Figure 3. Maturation of TDP-43 liquid droplets is detected as oligomerization by SDD-AGE. *A*, representative microscope images of fluorescently labeled TDP-43 (0.5 μM) LLPS. Liquid droplets formed in low salt (50 mM NaCl) but not in high salt (250 mM NaCl). Incubation of samples for 30 min or longer at 22 °C resulted in fibril-like structures. *Scale bar*, 2 μm. *B*, the number of droplets formed at 50 and 250 mM NaCl were quantified by ImageJ ($n = 3$, S.E.). *C*, samples in low and high salt conditions analyzed by SDD-AGE/immunoblot and compared with 0 and 10 day aggregates (*Aggr.*). LLPS samples at low and high salt analyzed after prolonged incubation (2 h). Microscope images and blots probed with TDP-43 antibody and are representative of more than three individual experiments.

Role of liquid–liquid phase transitions in oligomer formation

RNA-binding proteins associated with ALS/FTD, including TDP-43, FUS, TIA-1, Matrin 3, and hnRNP A1 undergo a process of condensation through liquid–liquid phase separation (LLPS) according to *in vitro* and in cell-based evidence (44). This activity mediates the formation of membraneless RNA-protein rich organelles in the nuclear and cytoplasmic cellular compartments (*e.g.* nucleoli and stress granules) (12, 45–47). Liquid droplets assembled through LLPS "mature" over time into solid-like complexes such as fibrils. Importantly, disease-linked conditions are proposed to disrupt LLPS and RNA granule assembly, thereby promoting aggregation and neurotoxicity in ALS and FTD (48–50). Therefore, self-assembly of these ALS and FTD-associated proteins is central to their physiological function but also plays a major role in aggregate formation. The mechanisms connecting these processes of LLPS and aggregation remain poorly characterized.

We asked whether the oligomeric complexes seen at the initial time points in the TDP-43 aggregation assay represent assemblies formed by LLPS. Microscope visualization of fluorescently labeled rTDP-43 in low salt (25–50 mM NaCl) showed immediate phase separation and formation of droplets similar to those recently reported by Maharana *et al.* (54) (Fig. 3*A*). Droplet formation was salt-dependent because the number of

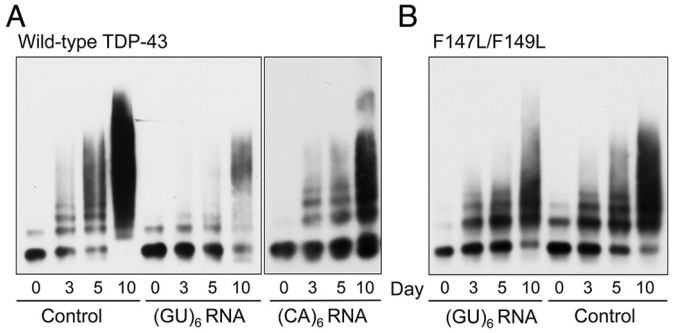

Figure 4. Specific binding of GU-rich RNA prevents TDP-43 aggregation. SDD-AGE/immunoblot analyses of TDP-43 aggregation over time in the presence and absence of 2′-*O*-methyl, phosphorothiorate-modified RNA (4 μM RNA and 2 μM protein). *A*, RNA composed of $(GU)_6$, $(CA)_6$ repeats, or control was added to rTDP-43 prior to triggering aggregation. *B*, aggregation of the RNA binding–deficient mutant F147L/F149L over time in the presence and absence of $(GU)_6$. All four blots were probed with TDP-43 antibody and are representative of more than individual experiments.

droplets was dramatically reduced at higher salt concentrations (250 mM), consistent with previous studies (Fig. 3*B*) (11, 47). Furthermore, phase separation was reversed by increasing the salt concentration to 250 mM, indicating that the observed complexes were not irreversible aggregates (data not shown). Interestingly, extending the incubation time of the sample beyond 30 min resulted in the growth of fibrillar structures as seen by fluorescence microscopy (Fig. 3*A*). We analyzed samples corresponding to those used for droplet formation at low and high salt and at longer incubation times by SDD-AGE (Fig. 3*C*). For control, we loaded samples from the aggregation assay days 0 and 10 (Figs. 1*A* and 2*A*). We found no macromolecular complexes by SDD-AGE in droplet conditions (25–50 mM NaCl) or at high salt (250 mM). However, incubation of the sample for 30 min to 2 h, parallel to the conditions that resulted in liquid droplet maturation, showed an increase in the oligomeric species similar to the pattern detected at the initial time points of the aggregation assay (Fig. 3*B*). These observations suggest that maturation of droplets into assemblies with solid-like properties may be detected by SDD-AGE and provide further evidence that the detergent-resistant oligomers form as the initial steps of misfolding and aggregation.

Specific binding to RNA rich in GU repeats decreases TDP-43 oligomer formation and aggregation

RNA is one of the principal physiological partners of TDP-43 mediating protein binding to hundreds of RNA transcripts. Genome-wide studies have shown a strong preference of TDP-43 for GU-rich sequences, an interaction of tight binding affinity (21, 51, 52). We tested whether RNA modulates the aggregation of rTDP-43 using our assay and focused on the effect of GU repeats. For these experiments we used 2′ *O*-methyl, phosphorothioate-modified RNA to reduce its degradation during the assay, at 2-fold molar excess of RNA to protein. We found that addition of $(GU)_6$ repeats strongly inhibited both the initial oligomerization and large aggregate formation of rTDP-43, compared with control (Fig. 4*A*). Significantly, $(GU)_6$ maintained higher levels of the monomer throughout the experiment. This was not observed when the protein was incubated with RNA composed of $(CA)_6$ repeats. To further test the role of specific RNA-binding interactions, we carried out similar aggregation assays with the RNA binding–deficient mutant F147L/F149L. Phe-147 and Phe-149 in the RNP1 motif of RRM1 make specific contacts with U and G bases, respectively (53), and double substitution of these amino acid residues (F147L/F149L) drastically decreases RNA binding (6, 21). We found that F147L/F149L oligomerization and aggregation resembles WT rTDP-43 but is not significantly affected by $(GU)_6$ RNA (Fig. 4*B*). Together, these experiments provide strong evidence that specific RNA binding stabilizes TDP-43 and prevents aggregation. This suggests that TDP-43 binding to target RNA transcripts, which are predominantly GU-rich sequences plays a major role in maintaining cellular TDP-43 homeostasis. Our results are in agreement with recent studies showing that RNA modulates LLPS and aggregation of RNA-binding proteins, proposing that RNA acts as a chaperone for this class of proteins (54).

Contribution of TDP-43 domains on protein assembly

To determine how each of the modular domains contributes to the two stages of assembly, we compared oligomer formation and aggregation of rTDP-43 deletion mutants (Fig. 5*A*). SDD-AGE analysis of the complexes showed that removal of the N-terminal domain (ΔN) decreased the formation of the initial oligomers and increased the formation of the large aggregates relative to the full-length protein (Fig. 5*B*). Conversely, deletion of the C-terminal low complexity region (ΔC) maintained the pattern of oligomerization and reduced the levels of large aggregates, consistent with its prion-like function. Removal of both N-and C-terminal domains (RRM1–2) triggered the formation of multiple oligomeric complexes starting at day 0 with little accumulation of high-molecular-weight species even after prolonged growth time. These results were supported by solubility assays in which protein samples (days 0 and 5 of the aggregation assay) were fractionated into RIPA-soluble and -insoluble fractions (Fig. 5*C*). The ratio of urea-soluble to RIPA-soluble protein was similar for all constructs at the initial time point (day 0). As expected, the later time point showed a significant increase of insoluble protein for full-length and ΔN (day 5) (Fig. 5, *C* and *D*). Deletion of the C-terminal low complexity domain reduced insoluble aggregates 6-fold compared with full-length TDP-43. The RRM1–2 fragment showed the highest solubility with little increase in the insoluble fraction over time (Fig. 5, *C* and *D*). These results suggest a strong contribution of RRM1–2 in TDP-43 oligomerization and that adding only the C-terminal domain in the absence of the entire N-terminal region accelerates large aggregate accumulation. This is consistent with the strong aggregation-prone characteristic of the C-tail (16–18).

Next, we investigated the structural changes associated with the different stages of TDP-43 aggregation seen by SDD-AGE using atomic force microscopy (AFM) and immuno-EM. Using these techniques, we studied both full-length TDP-43 and truncation mutants to compare the structure of large aggregates *versus* oligomeric patterns. AFM experiments showed that RRM1–2 does not form visible particles at day 0, whereas the full-length protein revealed small round oligomeric structures without incubation (Fig. 6*A*). After 1 day, the full-length formed

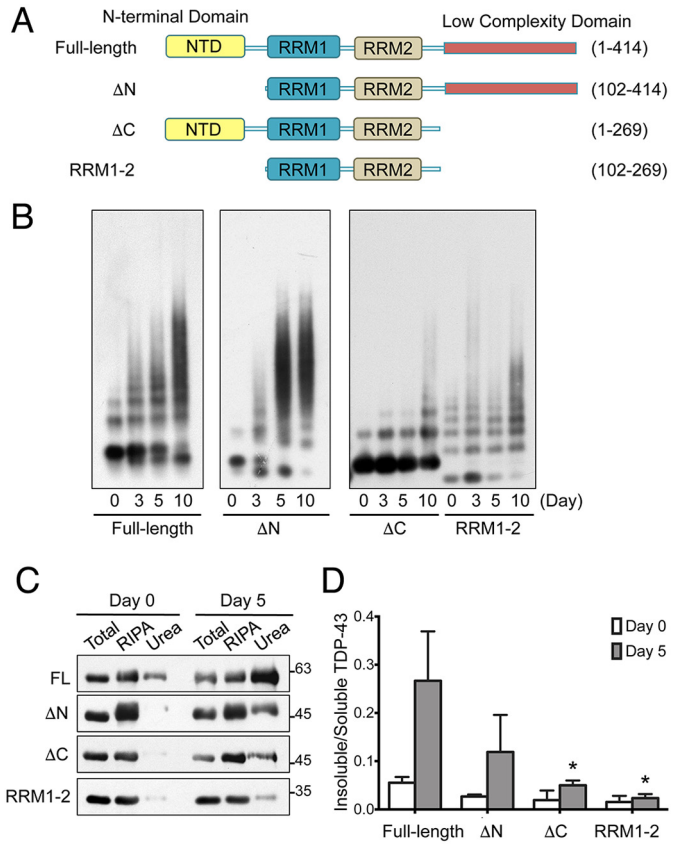

Figure 5. Role of TDP-43 protein domains in oligomerization and aggregate formation. *A*, schematic representation of TDP-43 deletion constructs devoid of N terminus (Δ*N*), C terminus (Δ*C*), or both (*RRM1–2*) consisting of the amino acid residues shown. *B*, aggregates formed by these protein fragments were analyzed by SDD-AGE/immunoblotting. Samples from *D*ays 0, 3, 5, and 10 were selected for comparison with full-length TDP-43. *C*, SDS-PAGE and immunoblotting of full-length rTDP-43 (*FL*) and deletion fragments fractionated into RIPA-soluble and -insoluble fractions. Insoluble pellets were resuspended in urea at days 0 and 5 of the aggregation assay. Equal volumes of starting lysate (*Total*) and RIPA-soluble fraction were loaded. Urea-soluble pellet represents 5-fold concentrated sample relative to RIPA-soluble fraction. *D*, RIPA and urea-soluble TDP-43 was quantified to compare the levels aggregation at the initial time point (day 0) and day 5 of the aggregation assay. Band intensity was quantified by ImageJ ($n = 3$, S.D.). The statistical significance (*, $p < 0.025$) comparing deletion fragments to full-length rTDP-43. All blots were probed with TDP-43 antibody and are representative of more than three individual experiments.

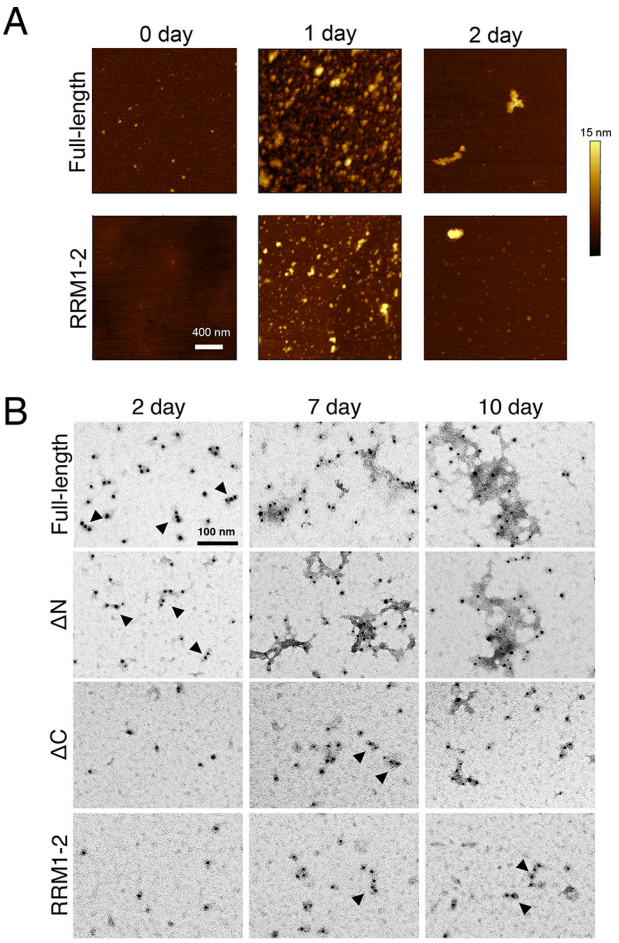

Figure 6. Oligomers are conformationally distinct from the large late-stage aggregates. Shown are structural analyses of full-length TDP-43 and deletion constructs during early (0, 1, and 2 days) and late assembly stages (7 and 10 days). *A*, representative atomic force microscopy image of full-length and RRM1–2 complexes at the earliest time points. *Scale bar*, 400 nm. *Z color bar*, 0–15 nm. *B*, immuno-EM of full-length, ΔN, ΔC, and RRM1–2 aggregates using TDP-43 antibody-coated gold particles. *Scale bar*, 100 nm. *Arrowheads* point to small complexes that are significantly smaller than the large fibril-like structures in full-length and ΔN day 7 and 10 samples.

larger density oligomers compared with RRM1–2. Nascent fibrillar structures of full-length rTDP-43 were observed after 2 days of incubation but were absent in RRM1–2 (Fig. 6*A*). Similarly, EM analysis showed fibrils of full-length TDP-43 at day 2, which grew in size after 7 and 10 days of incubation (Fig. 6*B*). This is consistent with previously obtained complexes formed by full-length TDP-43 and C-terminal domain protein fragments (27, 55). In contrast, aggregates of RRM1–2 and ΔC fragments appeared as smaller structures. Unlike full-length and ΔN aggregates, RRM1–2 and ΔC fragments failed to grow into large fibril-like assemblies by days 7 and 10. This is consistent with the assembly pattern of full-length and mutant rTDP-43 seen by SDD-AGE (Fig. 5*B*). Binding of anti-TDP-43 immunogold particles confirmed that the assemblies were formed by the respective proteins. Collectively, these results strongly suggest that the initial assembly during TDP-43 aggregation, which we detected as an ordered oligomeric pattern by SDD-AGE, are structurally different from later-day aggregates. The larger aggregates form fibril-like structures similar to those previously observed for full-length TDP-43 using similar microscopy methods (16, 55).

To further dissect the contribution of TDP-43 domains during the different stages of aggregation, we studied two additional mutations (Fig. 7*A*). We generated a mutant harboring double residue substitutions, Y4R/E17R, to address the role of N-terminally mediated assembly without deleting the entire N-terminal region. These mutations do not affect folding but disrupt N-terminal domain self-assembly *in vitro* and splicing regulatory function in cells (11). To confirm that Y4R/E17R disrupts self-assembly through the N-terminal domain, we studied its LLPS behavior. Compared with WT rTDP-43, Y4R/E17R showed a markedly reduced ability to form liquid droplets (Fig. 7*B*), in agreement with previous studies showing that TDP-43 LLPS decreases upon disruption of N-terminal domain-mediated association (11). The aggregation assays showed that Y4R/E17R did not affect oligomerization (Fig. 7*C*), suggesting that N-terminally mediated assembly does not play a

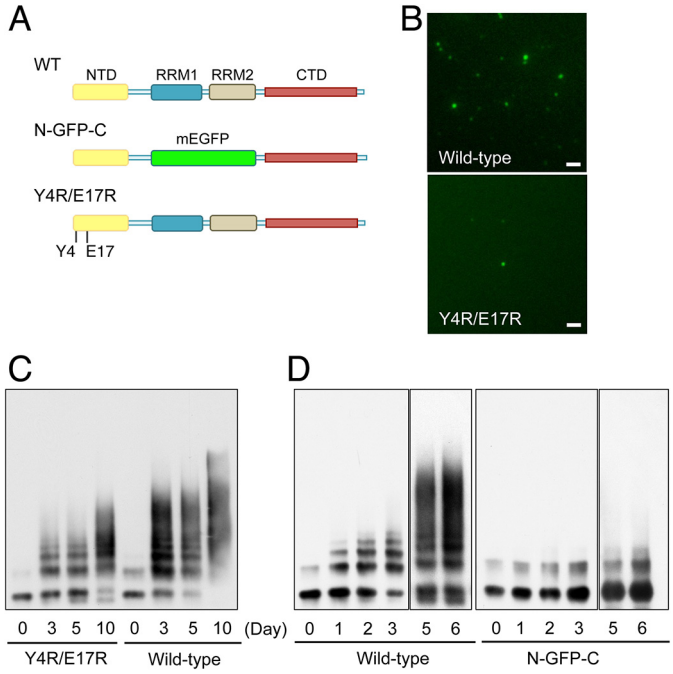

Figure 7. Full-length rTDP-43 oligomerization at the initial aggregation stage requires RRM1 and 2 but not N-terminal domain-driven assembly. *A*, schematic representation of the chimera construct replacing RRM1–2 with mEGFP (N-GFP-C) and double residue substitution at the N terminus, Y4R/E17R. *B*, representative microscope images of fluorescently labeled rTDP-43 comparing liquid droplet formation of WT and Y4R/E17R. *Scale bar*, 2 μm. *C*, SDD-AGE/immunoblot analyses of WT rTDP-43 and Y4R/E17R aggregates collected from days 0–10. *D*, WT rTDP-43 and N-GFP-C samples collected during the initial aggregation phase (days 0–6) analyzed by SDD-AGE. Immunoblots were probed with TDP-43 antibody and are representative of more than four individual experiments.

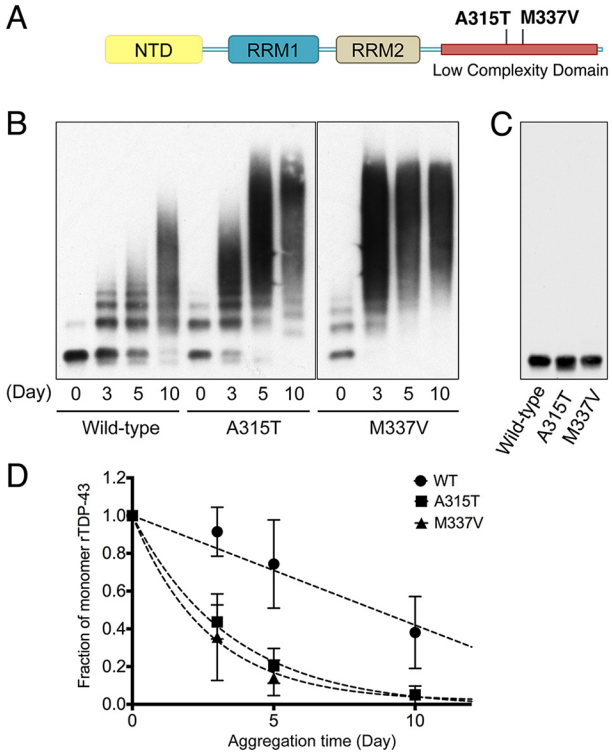

Figure 8. ALS mutations accelerate the rate of TDP-43 aggregation into high-molecular-weight aggregates. *A*, ALS-linked mutations A315T and M337V in the C-terminal domain of TDP-43 were analyzed by SDD-AGE/immunoblot. *B*, samples were shaken and collected immediately after (day 0) and after 3, 5, and 10 days. *C*, WT and mutant soluble protein samples collected prior to triggering aggregation. The blots were probed with TDP-43 antibody and are representative of more than three individual experiments. *D*, monomer, corresponding to the fastest migrating band, was quantified by ImageJ at the different time points for WT, A315T, and M337V. *Curves* were generated by fitting data points to an exponential formula in GraphPad Prism (n = 3, S.E.).

role in mediating the initial phase of TDP-43 aggregation. To address the role of RRM1–2 in the context of the full-length protein, we replaced the RNA-binding domains with monomeric EGFP (N-GFP-C) (Fig. 7*A*). We analyzed N-GFP-C aggregation focusing on the early days of the assay and found almost-complete inhibition of oligomerization with the chimera, compared with WT (Fig. 7*D*). Even at later time points, whereas WT rTDP-43 accumulated larger aggregates, N-GFP-C remained mostly monomeric. This provides strong evidence for the central role of RRM1 and 2 in the initial oligomerization during TDP-43 misfolding and confirms the results obtained with the RRM1–2 fragment (Fig. 5*B*). Moreover, the data showed that disruption of oligomer formation greatly delays aggregation in our assays. It is possible that inhibition of large aggregates in N-GFP-C were partially due to the loss of disulfide bonds and would be consistent with our results in Fig. 2*C*. The RRM1–2 region contains four of the six Cys residues in full-length TDP-43. This would suggest that oligomerization at the initial phase of TDP-43 aggregation creates a structural scaffold for high-molecular-weight aggregates and that this also depends on covalent disulfide bond formation. This model may be tested by analyzing the aggregation of mutants substituting RRM1–2 Cys residues to examine how these affect oligomer and large aggregate assembly. It is also possible that during misfolding, TDP-43 oligomerization and aggregation represent two alternative pathways that follow different assembly kinetics. This may be tested with additional TDP-43 variants that specifically stabilize or block oligomeric complexes.

Disease-linked mutations increase the assembly and aggregation of TDP-43 in vitro

The pathogenesis of ALS-causative mutations in TDP-43, for the most part, remains to be elucidated. Understanding how these mutations affect TDP-43 homeostasis and function is critical in uncovering the disease mechanisms of ALS and FTD. The clinicopathological features or TDP-43 lesions are similar in patients with or without TDP-43 mutations. This suggests that alternative methods are needed to understand the differences between WT and mutant TDP-43 at the molecular level. To test whether our assay may be used to determine how these mutations affect the aggregation process, we studied two single-site substitutions: A315T and M337V (Fig. 8*A*). Both mutations are highly associated with disease and previously reported to increase aggregation *in vitro* and promote neurotoxicity in animal models (5, 27, 56, 57). We performed aggregation assays with A315T and M337V and analyzed the complexes formed over time by SDD-AGE (Fig. 8*B*). We observed that both mutations potently impacted the rate of aggregation as seen by significantly accelerated oligomer formation at the earliest time point (day 0), which was mostly absent in WT. The oligomer pattern typical of days 3 and 5 in WT TDP-43 was substituted by the larger aggregates in the mutants, particularly in the case of M337V. We also analyzed the initial soluble samples by SDD-

AGE to examine whether or not oligomers were already present before triggering aggregation. Fig. 8*C* shows that oligomers or aggregates are absent from the starting WT and mutant samples. Quantifying aggregation rates from the loss of monomer protein at different time points showed that although WT monomer decreased linearly as a function of time, A315T and M337V monomers decreased at a significantly faster exponential rate (Fig. 8*D*). This, particularly the effect of M337V, is in strong agreement with previous observations that these substitutions increase amyloid formation of the isolated disordered C-tail (58, 59) and full-length protein (16) and disrupt phase separation in cell models (60–62). Our results on the macromolecular assembly of A315T and M337V may reflect distinct structures formed in the presence of the substitutions that have faster rates of complex association. Alternatively, these results may suggest that disease mutations decrease the dissociation of TDP-43 molecules making more stable complexes that result in stable fibrils or aggregates.

rTDP-43 aggregates seed and propagate intracellularly and this is enhanced by ALS mutations

Propagation of aggregates through prion-like transcellular transmission has been documented for a number of proteins associated with neurodegeneration, including TDP-43 (63, 64). Previous studies showed TDP-43 seeding in cells; however, these assays used TDP-43 protein fragments, and the resulting intracellular aggregates were not detected by established markers of TDP-43 pathology, *i.e.* phosphorylation at Ser-409/410 (65–67). To investigate the aggregate seeding function of our rTDP-43 aggregates in cells, we generated a stable cell line to detect cytoplasmic aggregates in a reproducible and sensitive assay. A single copy of mCherry-tagged TDP-43 was stably integrated in HEK293 cells for tetracycline-induced expression (HEK-TDP-43^{NLS}) (Fig. S4). This facilitated visualization of TDP-43 and prevented high and nonhomogeneous levels of transgene overexpression that could disrupt protein homeostasis. This system offers an advantage to studying TDP-43 aggregation relative to transient transfection, which often causes overexpression of the protein. We expressed full-length TDP-43^{NLS} harboring alanine substitutions disrupting the nuclear localization signal (NLS) and increasing cytoplasmic TDP-43, as previously observed (68, 69) (Fig. S4, *A* and *B*). Expression of a similar TDP-43 NLS-mutant causes neurotoxicity accompanied by pathological inclusions in brain and spinal cord in mice (70). Our HEK-TDP-43^{NLS} cells expressed soluble TDP-43^{NLS} under control conditions but could be induced to form cytoplasmic aggregates readily detected by microscopy after addition of proteotoxic agents (*e.g.* MG132 and sodium arsenite) (Fig. S4, *B* and *E*). We confirmed that the cytoplasmic inclusions triggered by proteotoxic stress were recognized by an antibody recognizing phosphorylated Ser-409/410 (Fig. S4, *C* and *D*).

We used lipofection-mediated transduction of rTDP-43 aggregates in HEK-TDP-43^{NLS} and observed protein internalization with fluorescently labeled rTDP-43. The protein was labeled with Oregon Green before initiating the aggregation assays. rTDP-43 samples collected shortly after triggering aggregation (day 0) (Fig. 1*A*) were delivered into cultured HEK-TDP-43^{NLS}. The cells were trypsinized and replated 24 h post-transfection to remove rTDP-43 from the medium and from association with the extracellular membrane. We observed internalization of labeled rTDP-43 48 h post-transfection (Fig. 9*A*). Aggregate formation of mCherry-TDP-43^{NLS} was monitored for several days. We observed a significant increase in cellular TDP-43 aggregation after 6 days of treatment, as seen by formation of large mCherry cytoplasmic foci (Fig. 9*A*). The mCherry-positive inclusions colocalized with the Oregon Green signal, suggesting the nucleation of *de novo* cellular aggregation by the rTDP-43 internalized aggregates. Cells treated with rTDP-43 aggregates showed a significant 2-fold increase in cells positive for mCherry aggregates compared with those treated with soluble rTDP-43 or no protein control (Fig. 9*B*). During our initial experiments, we tested seeding activity using rTDP-43 aggregates collected at various time points (0, 3 and 10 day aggregates). We did not find significant differences in the levels of rTDP-43 internalization or aggregate seeding between rTDP-43 aggregates collected at different time

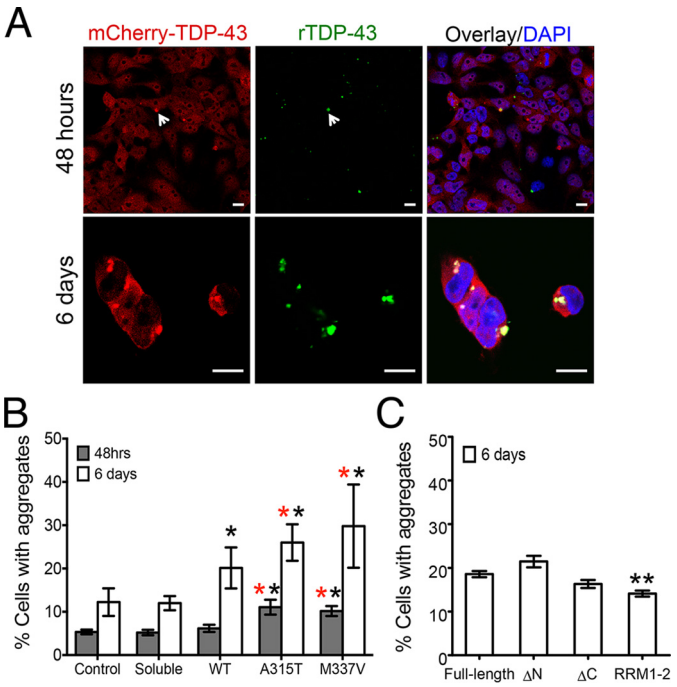

Figure 9. Intracellular TDP-43 aggregate seeding increases with disease-linked mutations but is reduced upon deletion of both N- and C-terminal domains. *A*, Oregon Green–labeled rTDP-43 aggregates, corresponding to day 5 in the aggregation assay, transfected in mCherry-TDP-43 expressing cells (HEK-TDP-43^{NLS}). The cells were trypsinized 24 h post-transfection, and rTDP-43 aggregate internalization was monitored 48 h post-transfection (*top panel*). *Arrowhead* points to colocalization of Green aggregates with mCherry-TDP-43 aggregates in the cytoplasm. *Bottom row*, mCherry-tagged TDP-43^{NLS} cellular aggregates visualized by microscopy at higher magnification after 6 days of treatment. Overlay shows additional merging with DAPI. *Scale bar*, 10 μm. *B*, the percentage of HEK-TDP-43^{NLS} cells showing cytoplasmic aggregates (mCherry-positive) was quantified after 48 h and 6 days of transfection with rTDP-43, including WT rTDP-43 aggregates (WT) and ALS mutant rTDP-43 aggregates (A315T and M337V). No protein and soluble WT rTDP-43 transfection was used as control. Statistical significance was calculated for control *versus* WT, A315T, and M337V at 48 h and 6 days (*black asterisk*); WT *versus* A315T and M337V at 48 h and 6 days (*red asterisk*) (>200 cells/sample counted in $n > 3$, S.D., GraphPad Prism two-tailed *t* test analysis; *black asterisk* and *red asterisk*, $p \leq 0.04$). *C*, percentage of HEK-TDP-43^{NLS} cells with mCherry-positive cytoplasmic aggregates quantified 6 days after transfection with full-length rTDP-43 and truncation mutant ΔN, ΔC, and RRM1–2 aggregates. Statistical significance calculated with >200 cells/sample, $n > 3$, S.D., using GraphPad Prism two-tailed *t* test analysis (*two black asterisks*, $p \leq 0.004$).

points (data not shown). The cellular aggregates were also positive for pSer-409/410 (Fig. S5, *A* and *B*), suggesting that the inclusions share structural and mechanistic similarities with those formed in disease. The relevance of our cellular reporter to study TDP-43 aggregate seeding is further supported by recent work using a similar HEK293 GFP-tagged TDP-43^{NLS} stable cell line (71). FTD-derived extracts positive for TDP-43 pathology showed cytoplasmic aggregate seeding in these cells and were also capable of propagating TDP-43 pathology in an *in vivo* model upon intracerebral injection in mice.

Next, we analyzed whether the ALS/FTD-linked mutations altered aggregate formation in cells as seen in our *in vitro* assays. Transduction of HEK-TDP-43^{NLS} with A315T and M337V rTDP-43 day 0 aggregates showed a significant 2-fold increase in mCherry-positive inclusions already at 48 h (Fig. 9*B*), whereas WT rTDP-43 aggregates did not show a significant difference compared with control at this time point. The effect of the disease-associated mutations was even greater after 6 days, showing a 3-fold increase in mCherry-TDP-43^{NLS} aggregates compared with control (Fig. 9*B*). A315T and M337V also caused significantly greater intracellular aggregation compared with WT, 50 and 67% increase, respectively, 6 days post-transfection. Of note, cellular internalization of rTDP-43 aggregates was similar for WT and mutant, and ~40% of cells showed cytoplasmic labeled rTDP-43. These results strongly suggest that the mutants do not alter cellular uptake but are more efficient at seeding and propagating relative to WT. This is in agreement with the increased rate of large aggregate assembly seen by SDD-AGE *in vitro* (Fig. 8*B*).

Similar experiments were performed with aggregates derived from rTDP-43 truncated mutants, ΔN, ΔC, and RRM1–2 to examine the contribution of oligomers *versus* large aggregates in cellular aggregate seeding. Deletion of both N- and C-terminal domains showed significantly reduced seeding function compared with WT. The proportion of cytoplasmic inclusions at 6 days post-transduction was similar (14%) in cells treated with RRM1–2 aggregates, soluble rTDP-43, or no protein control (Fig. 9, *B* and *C*). The seeding function of ΔN and ΔC were not statistically significantly different from full-length aggregates but showed increased and reduced mCherry-positive aggregates, respectively. Collectively, these results suggest that the oligomeric intermediates are not sufficient to nucleate cytoplasmic TDP-43 aggregation in the absence of the N terminus and particularly, upon deletion of the C-terminal region. Additional studies are needed to determine whether preventing oligomerization in the context of full-length TDP-43 disrupts aggregate seeding function.

Discussion

Our studies shed new light into the molecular steps that lead to TDP-43 aggregation and highlight methods to study the factors that control TDP-43 proteostasis and/or trigger protein misfolding. We also report a previously unappreciated role for disease-associated mutations on the aggregation mechanisms, providing important clues on how these mutations lead to pathology.

The use of SDD-AGE to analyze rTDP-43 aggregates provided the first evidence of a defined oligomeric pattern that precedes formation of TDP-43 high-molecular-weight aggregates (Figs. 1*A* and 2*A*). These intermediates may not be observed by other methods used to monitor aggregation, such as turbidity and other spectroscopic techniques. We confirmed the differences in the conformation and assembly state of early- and late-stage aggregates by AFM/immuno-EM analysis (Fig. 6). Interestingly, our findings suggest that the oligomers detected by SDD-AGE are key intermediates during the transition from liquid droplets to irreversible aggregates (Fig. 3). This is consistent with the model that TDP-43 liquid–liquid phase separation may lead to aggregation over time, as suggested by studies of similar RNA-binding proteins linked to ALS/FTD (48, 50). This mechanism resembles the aggregation process of other neurotoxic proteins, such as Tau, α-synuclein, and β-amyloid, in which these intermediate products have been proposed to be the toxic seeds that transmit cell damage and pathology (72–78). Future experiments will examine whether the TDP-43 oligomers at the initial aggregation time points are also more toxic to cells and/or propagate more efficiently than large aggregates in animal models.

The mechanisms and structural determinants of TDP-43 oligomerization have not been widely reported, although strong evidence supports TDP-43 physiological oligomerization in cells and in brain tissue (9, 27, 37). The initial complexes we observe in our aggregation assays represent at least partially misfolded species that may act as precursors of protein aggregation. These are likely to be different from the soluble assemblies formed in cells, which would be expected to disassemble under the semi-denaturing conditions used for SDD-AGE analysis. Our SDD-AGE results showing that the size and levels of oligomeric complexes increase at higher temperatures further suggest that these form as the protein undergoes misfolding (Fig. 2*A*). Based on our findings, TDP-43 shows key similarities with the canonical yeast prion protein Sup35, which was recently found to assemble into functional, soluble complexes through liquid–liquid phase separation *in vitro* and in yeast models (79). However, Sup35 also forms partially SDS-resistant oligomers that promote prion propagation (80).

Our observation that aggregates generated from the purified protein seed cellular cytoplasmic inclusions (Fig. 9) are consistent with previous reports and our own observations (data not shown) that TDP-43 aggregates from disease tissue and isolated TDP-43 C-terminal fragments promote cellular TDP-43 aggregation (41, 64, 81) and more recently in mouse brain (71). Moreover, these results show that rTDP-43 aggregates are relevant to cell and patient-derived inclusions and suggest that, similar to Tau and α-synuclein, TDP-43 aggregates act as templates in cellular TDP-43 aggregation (63). We also provide strong evidence that enhanced TDP-43 aggregation rates translate into greater cellular seeding function, as seen with the ALS-linked mutations A315T and M337V. By studying the aggregation and seeding of A315T and M337V, we propose that pathogenesis is strongly influenced by factors that increase the assembly and/or alter the dissociation rates. Changes in the aggregation rate may be due to structurally distinct complexes associated with the mutations. However, our observations that A315T and M337V aggregates nucleate cellular TDP-43 suggest that mutant complex structure and assembly pathways are sufficiently similar to

WT to act as seeds for aggregation. These findings open the avenue for future studies aimed at addressing whether the mechanisms observed with A315T and M337V apply to other TDP-43 disease-associated mutations. This will increase our understanding of the molecular basis of ALS-FTD pathogenesis. Importantly, studies on the mechanisms by which these mutations alter structural and kinetic parameters of TDP-43 self-assembly will shed light on the regulation of the equilibrium between soluble complexes and irreversible aggregates.

Until recently, most efforts to understand TDP-43 aggregation centered on the low complexity C-terminal region. Our results provide strong evidence supporting a central role of the RNA-binding domains in TDP-43 aggregation, particularly during the initial phase of misfolding. We showed that replacing both RRMs with monomeric GFP drastically disrupts oligomerization and reduces large aggregate accumulation over time (Fig. 7*D*). First, this suggests that in the absence of the RRM-dependent oligomers, the N terminus and the C-tail are not sufficient to form detergent-resistant aggregates, which share common features with FTD and cell-derived inclusions (Fig. 1, *B* and *C*). Second, it supports a model in which oligomerization provides a scaffold for TDP-43 aggregation. Previous studies showed that isolated RRM2 forms aggregates (82) and that RRM2 polypeptides that are normally buried under native conditions assemble into amyloid, leucine zipper structures (83–86). Based on these previous findings and our results, we predict that RRM2 forms a hydrophobic core, intermediate structure upon TDP-43 unfolding that mediates the oligomers detected by SDD-AGE. Interestingly, the strong effect of RNA binding in preventing TDP-43 oligomerization and aggregation (Fig. 4) provides further support that stabilizing a specific RRM conformation maintains protein solubility.

Experimental procedures

All reagents are from Sigma–Aldrich unless otherwise specified.

Plasmid construction

Construction of the TDP-43 vector for bacterial expression (SUMO-TDP43) was previously described (21). Oligonucleotides used for mutagenesis and cloning are described in Table S1. Deletion constructs for bacterial expression were made by standard PCR and cloning between BamHI and SacI restriction sites in pET28b/His-SUMO (87). Single-site substitutions, including modification of the TDP-43 nuclear localization sequence, were made by site-directed mutagenesis using the QuikChange site-directed mutagenesis kit (Agilent Technologies) as described (15). The template used for mutagenesis of the mammalian expression vector, HA-mCherry-TDP-43, was made by cloning hemagglutinin peptide-mCherry cDNA into pCDNA5/FRT upstream of TDP-43 cDNA (NM_007375.3). TDP-43 was cloned between BamHI and NotI sites. N-GFP-C was generating by PCR-mediated fusion of TDP-43 residues 2–101, mEGFP, and TDP-43 residues 261–414. This chimera was cloned between BamHI and SacI restriction sites in pET28b/His-SUMO.

Recombinant TDP-43 production and aggregation assays

Recombinant TDP-43 (rTDP-43) was generated in *Escherichia coli* and purified as previously described (21). His-tagged recombinant Ulp1 protease was used to remove SUMO. Briefly, rTDP-43 in the expression lysate was bound to nickel–nitrilotriacetic acid–agarose and washed with wash buffer 1 (50 mM Tris, pH 8.0, 500 mM NaCl, 10% glycerol, 10% sucrose, 1 mM TCEP), washed with wash buffer 2 (50 mM Tris, pH 8.0, 500 mM NaCl, 10% glycerol, 10% sucrose, 50 mM Ultrol Grade imidazole, pH 8.0, 1 mM TCEP), and finally washed again with wash buffer 1 to remove imidazole. Ulp1 was added to the protein-bound beads at an approximate 1:1 molar ratio and incubated for 30 min at 22 °C. The supernatant containing cleaved TDP-43 was collected. For the aggregation assays rTDP-43 was ultracentrifuged in a Beckman Coulter Optima TLX Ultracentrifuge using a TLA55 rotor at 40,000 rpm for 30 min at 4 °C to remove any pre-existing aggregates. Soluble protein concentration was measured by nanodrop and diluted to 2 μM in the reaction buffer (50 mM Tris, pH 8.0, 250 mM NaCl, 5% glycerol, 5% sucrose, 150 mM Ultrol Grade imidazole, pH 8.0). rTDP-43 aggregation was started by shaking at 1,000 rpm at 22 °C for 30 min with an Eppendorf ThermoMixer C. Samples were incubated at 22 °C and collected for analysis by adding equal volume of 2× SDD-AGE sample buffer (80 mM Tris-HCl, pH 6.8, 10% glycerol, 1% SDS, 0.2% bromphenol blue) and incubated at 22 °C for 10 min prior to loading on SDD-AGE. Analysis of rTDP-43 aggregates was performed by SDD-AGE as previously described (24, 28), on a horizontal 1.5% agarose gel electrophoresis in 20 mM Tris, 200 mM glycine, and 0.1% SDS. Proteins were transferred onto polyvinylidene difluoride membrane (Amersham Biosciences Hybond 0.45 μm polyvinylidene difluoride; GE Healthcare) in a modified Mini Trans-Blot cell (Bio-Rad) at 4 °C. Protein was detected with traditional immunoblotting.

Sequential extraction of TDP-43 from postmortem human brain tissue

Samples of frozen postmortem human brain tissue from control and FTD deidentified cases were obtained from the Cognitive Neurology and Alzheimer's Disease Center at Northwestern University. Gray matter was dissected from frontal cortex samples using a scalpel while maintaining the tissue in a frozen state. Extraction methods were adapted from (33). Samples of dissected tissue (~100 mg) were homogenized in 5 ml/g Tris-sucrose buffer (25 mM Tris-HCl, pH 7.4, 5 mM EDTA, 1 mM DTT, 10% sucrose, protease inhibitor (PI) mixture) with Kontes Dounce tissue grinders (Kimble KT885300-0002). The homogenate was spun at 18,000 × *g* (average relative centrifugal force) for 30 min at 4 °C. The resulting pellet was next extracted in 5 ml/g Triton X-100 buffer (Tris sucrose buffer, 1% Triton X-100, 0.5 M NaCl) and centrifuged at 135,000 × *g* (RCF average) for 30 min at 4 °C. To float and remove myelin, the pellet was further extracted in TX-30% sucrose buffer (25 mM Tris-HCl, pH 7.4, 5 mM EDTA, 1 mM DTT, 10% sucrose, 1% Triton X-100, 0.5 M NaCl, 30% sucrose, PI mixture) and centrifuged at 135,000 × *g* (RCF average) for 30 min at 4 °C. Finally, the pellet was homogenized in 5 ml/g sarkosyl buffer (25 mM Tris, pH 7.4,

5 mM EDTA, 1 mM DTT, 10% sucrose, 1× PI mixture, 1% *N*-lauroylsarcosine sodium salt, 0.5 M NaCl) and incubated at room temperature for 1 h with shaking at 750 rpm on Advanced Vortex Mixer (VWR 89399-884). The sarkosyl extracted homogenate was centrifuged at 135,000 × *g* (RCF average) for 30 min at 4 °C. The resulting pellet was resuspended in 100 μl of RIPA buffer (50 mM Tris, pH 8.0, 150 mM NaCl, 1% Nonidet P-40, 0.5% SDC, 0.1% SDS, 5 mM EDTA, PI mixture, PhosStop (Roche)), sonicated with a nanoruptor (Diagenode) for 10 cycles of 30 s on, 30 s off. SDD-AGE analysis was carried out with 25 μl of this sample, representing 12.5% of the initial sample.

Thioflavin binding

To test binding of initial rTDP-43 aggregates to the amyloid-detection dye, ThioT, rTDP-43 monomer was first spun down at 100,000 × *g* for 30 min at 4 °C to remove any aggregates formed during the freeze–thaw process. In a Corning Black 96-well plate (Fisher, catalog no. 07-200-762), 50 μl of 0.5 μM rTDP-43 monomer was combined with increasing concentrations (0–1000 nM) of ThioT in a final volume of 100 μl. Nonspecific signal was assessed by incubating ThioT alone with buffer. The reaction mixture was incubated for 2 h at room temperature to allow formation of rTDP43 aggregates. At the end of incubation, ThioT fluorescence was measured in a BioTek plate reader using a 440/30-nm excitation filter, a 485/20-nm emission filter, and top 50% optical setting. In parallel, we incubated 0.5 μM of recombinant α-synuclein fibrils with ThioT under the same conditions used for rTDP43. Methods to produce recombinant α-synuclein monomer and fibrils were as described previously (38). ThioT and ThioS binding to TDP-43 cellular aggregates was performed using HEK-TDP-43^{NLS} cells treated with sodium arsenite (0.5 mM, 30 min). Binding was analyzed by immunofluorescence of paraformaldehyde-fixed cells using 1 mM dye.

Liquid–liquid phase separation assays

Oregon Green 488–labeled rTDP-43 was mixed with unlabeled protein at a 1:10 ratio at 0.5 μM in 18 mM MES, pH 7.0, 5 mM Tris, 50 mM NaCl, 1% glycerol, 1% sucrose, 30 mM imidazole. The samples were visualized by fluorescence microscopy immediately or incubated at 22 °C for 30–120 min prior to analysis or SDD-AGE. Reversal of phase separation was achieved by raising the NaCl concentration to 250 mM immediately after droplet formation.

Insoluble/soluble fractionation of rTDP-43 proteins

Samples were collected after ultracentrifugation as above (day 0) or shaken for 30 min and collected after 5 days of incubation at 22 °C (day 5). The samples were sonicated in a Bioruptor Pico (Diagenode) (30 s on/30 s off, 10 cycles) and ultracentrifuged at 40,000 rpm for 30 min at 4 °C, and soluble fraction was obtained. The insoluble pellet was washed with RIPA-50 buffer (50 mM Tris, pH 8.0, 150 mM NaCl, 1% nonylphenylpolyethylene glycol (Nonidet P-40), 10 mM EDTA, 0.5% SDC, and 0.1% SDS), sonicated, and ultracentrifuged. The remaining insoluble pellet was resuspended in urea buffer (30 mM Tris, pH 8.8, 7 M urea, 2 M thiourea, and 4% CHAPS).

Cross-linking and labeling rTDP-43

For cross-linking analysis, rTDP-43 (0.5 or 1 μM) was incubated with 0.25 mM disuccinimidyl suberate (Thermo Scientific) for 1 h at 22 °C. The reaction was quenched by addition of Tris, pH 8.0, to 50 mM final concentration and incubated for 15 min at 22 °C. rTDP-43 the was labeled with Oregon Green 488 maleimide (ThermoFisher Scientific) according to manufacturer's protocol. Labeled protein was purified with ZebaSpin columns (ThermoFisher Scientific) and used to label aggregates. Aggregation or LLPS assays included a 1:10 ratio mixture of labeled to nonlabeled rTDP-43.

Atomic force and immuno-EM

Aliquots of rTDP-43 aggregation time points (10 μl) were placed on a clean, freshly cleaved grade V-1 mica (catalog no. 01792-AB, Structure Probe, Inc.). After 10 min, the solvent was wicked off by filter paper, and the mica was washed six times with 20 μl of water to remove salts and buffer from the sample. Samples were dried overnight, and AFM images were acquired in tapping mode on a Veeco Dimension 3100 machine (Bruker) with Bruker FESP tips. AFM images were analyzed using the Gwyddion SPM data visualization tool. Carbon films on 200-mesh copper grids (Ted Pella) were incubated with 5 μl of sample in the dark side of the grid. After 10 min, the sample was wicked off from the grid and was incubated with 10 μl, 1% BSA in PBS to block any nonspecific binding. The grid was incubated with primary rabbit TDP-43 antibody 1:100 diluted in PBS solution containing 0.1% BSA for 45 min. The grid was then washed by seven drops of PBS buffer. The grid was incubated with secondary anti-rabbit IgG antibody conjugated to 5-nm-diameter gold nanoparticles (Sigma–Aldrich) diluted 1:20 in PBS buffer containing 0.1% BSA. 45 min later, the grid was washed by seven drops of PBS followed by seven drops of water. Finally, the grid was stained by 4% uranyl acetate solution for 10 min, washed with seven drops of water, and air-dried before collecting the images on a JEM-1400 Plus transmission electron microscope.

Cell culture

The cells were grown in growth medium–Dulbecco's modified Eagle's medium, 4,500 mg/liter glucose, L-glutamine, and sodium bicarbonate and supplemented with filtered fetal bovine serum at 10%. The cells were incubated at 37 °C, 5% CO_2. Stable human embryonic kidney cells expressing TDP-43^{NLS} (HEK-TDP-43^{NLS}) upon induction with tetracycline were generated from Flp-In™T-REX™293 cells (ThermoFisher) according to the manufacturer's instructions. The cells were grown in the presence of hygromycin (50 μg/ml), and transgene expression was induced with 1 μg/ml tetracycline.

TDP-43 aggregate cellular seeding

HEK-TDP-43^{NLS} were plated and induced with 1 μg/ml tetracycline for 16 h to reach 80–90% confluency. Recombinant TDP-43, day 0 aggregates were transduced with Pierce protein transfection reagent according to the manufacturer's instructions at a final protein concentration of 0.1 μM in the culture media. As controls, soluble rTDP-43 or transfection reagent

only were used. The medium was changed 6 h post-transfection. After 24 h, the cells were trypsinized, washed, and replated. For immunofluorescence, the cells were plated on poly-D-lysine–coated coverslips 48 h prior to fixation in 4% paraformaldehyde for 20 min. For fluorescence microscopy, slides were permeabilized for 5 min at 4 °C with 0.3% Triton X-100 and DAPI-stained. Coverslips were mounted, and the cells were observed on a Leica DMI3000B inverted microscope and Leica AF6000E software (Leica Microsystems Inc.). A 63×/1.4 oil immersion objective was used for confocal microscopy studies on a TCS SP5 microscope (Leica) using the LAS AF software. Images were taken with the DAPI filter to eliminate bias selection of aggregates. Cells positive for cytoplasmic aggregation were quantified using ImageJ.

Antibodies

Immunoblots and indirect immunofluorescence were performed with rabbit polyclonal anti–TDP-43 (ProteinTech 10782-2-AP), anti–TDP-43 phosphorylated at Ser-409/410 (Cosmo Bio, CAC-TIP-PTD-M01), and horseradish peroxidase–conjugated goat anti-rabbit (Fisher Scientific PI-31460).

Author contributions—R. L. F., Z. R. G., H. A., D. D. D., A. N. R., and N. K. investigation; R. L. F., D. D. D., J. B., and Y. M. A. writing-review and editing; D. D. D., P. T. K., and J. B. methodology; Y. M. A. conceptualization; Y. M. A. formal analysis; Y. M. A. supervision; Y. M. A. funding acquisition; Y. M. A. writing-original draft; Y. M. A. project administration.

Acknowledgments—We thank the Cognitive Neurology and Alzheimer's Disease Center at Northwestern University and Eileen Bigio for providing the patient tissue; Heather True-Krob and lab members for help in setting up SDD-AGE assays; and Alessandro Vindigni for careful and critical reading of our manuscript.

References

1. Neumann, M., Sampathu, D. M., Kwong, L. K., Truax, A. C., Micsenyi, M. C., Chou, T. T., Bruce, J., Schuck, T., Grossman, M., Clark, C. M., McCluskey, L. F., Miller, B. L., Masliah, E., Mackenzie, I. R., Feldman, H., *et al.* (2006) Ubiquitinated TDP-43 in frontotemporal lobar degeneration and amyotrophic lateral sclerosis. *Science* **314,** 130–133 CrossRef Medline
2. Arai, T., Hasegawa, M., Akiyama, H., Ikeda, K., Nonaka, T., Mori, H., Mann, D., Tsuchiya, K., Yoshida, M., Hashizume, Y., and Oda, T. (2006) TDP-43 is a component of ubiquitin-positive tau-negative inclusions in frontotemporal lobar degeneration and amyotrophic lateral sclerosis. *Biochem. Biophys. Res. Commun.* **351,** 602–611 CrossRef Medline
3. Uryu, K., Nakashima-Yasuda, H., Forman, M. S., Kwong, L. K., Clark, C. M., Grossman, M., Miller, B. L., Kretzschmar, H. A., Lee, V. M., Trojanowski, J. Q., and Neumann, M. (2008) Concomitant TAR–DNA–binding protein 43 pathology is present in Alzheimer disease and corticobasal degeneration but not in other tauopathies. *J. Neuropathol. Exp. Neurol.* **67,** 555–564 CrossRef Medline
4. Josephs, K. A., Whitwell, J. L., Weigand, S. D., Murray, M. E., Tosakulwong, N., Liesinger, A. M., Petrucelli, L., Senjem, M. L., Knopman, D. S., Boeve, B. F., Ivnik, R. J., Smith, G. E., Jack, C. R., Jr., Parisi, J. E., Petersen, R. C., *et al.* (2014) TDP-43 is a key player in the clinical features associated with Alzheimer's disease. *Acta Neuropathol.* **127**, 811–824 CrossRef Medline
5. Buratti, E. (2015) Functional significance of TDP-43 mutations in disease. *Adv. Genet.* **91,** 1–53 CrossRef Medline
6. Buratti, E., and Baralle, F. E. (2001) Characterization and functional implications of the RNA binding properties of nuclear factor TDP-43, a novel splicing regulator of CFTR exon 9. *J. Biol. Chem.* **276,** 36337–36343 CrossRef Medline
7. Ayala, Y. M., Pantano, S., D'Ambrogio, A., Buratti, E., Brindisi, A., Marchetti, C., Romano, M., and Baralle, F. E. (2005) Human, *Drosophila*, and *C. elegans* TDP43: nucleic acid binding properties and splicing regulatory function. *J. Mol. Biol.* **348,** 575–588 CrossRef Medline
8. D'Ambrogio, A., Buratti, E., Stuani, C., Guarnaccia, C., Romano, M., Ayala, Y. M., and Baralle, F. E. (2009) Functional mapping of the interaction between TDP-43 and hnRNP A2 *in vivo*. *Nucleic Acids Res.* **37,** 4116–4126 CrossRef Medline
9. Afroz, T., Hock, E. M., Ernst, P., Foglieni, C., Jambeau, M., Gilhespy, L. A. B., Laferriere, F., Maniecka, Z., Plückthun, A., Mittl, P., Paganetti, P., Allain, F. H. T., and Polymenidou, M. (2017) Functional and dynamic polymerization of the ALS-linked protein TDP-43 antagonizes its pathologic aggregation. *Nat. Commun.* **8,** 45 CrossRef Medline
10. Mompeán, M., Romano, V., Pantoja-Uceda, D., Stuani, C., Baralle, F. E., Buratti, E., and Laurents, D. V. (2017) Point mutations in the N-terminal domain of transactive response DNA-binding protein 43 kDa (TDP-43) compromise its stability, dimerization, and functions. *J. Biol. Chem.* **292,** 11992–12006 CrossRef Medline
11. Wang, A., Conicella, A. E., Schmidt, H. B., Martin, E. W., Rhoads, S. N., Reeb, A. N., Nourse, A., Ramirez Montero, D., Ryan, V. H., Rohatgi, R., Shewmaker, F., Naik, M. T., Mittag, T., Ayala, Y. M., and Fawzi, N. L. (2018) A single N-terminal phosphomimic disrupts TDP-43 polymerization, phase separation, and RNA splicing. *EMBO J.* **37,** e97452 CrossRef Medline
12. Kato, M., Han, T. W., Xie, S., Shi, K., Du, X., Wu, L. C., Mirzaei, H., Goldsmith, E. J., Longgood, J., Pei, J., Grishin, N. V., Frantz, D. E., Schneider, J. W., Chen, S., Li, L., Sawaya, M. R., *et al.* (2012) Cell-free formation of RNA granules: low complexity sequence domains form dynamic fibers within hydrogels. *Cell* **149,** 753–767 CrossRef Medline
13. King, O. D., Gitler, A. D., and Shorter, J. (2012) The tip of the iceberg: RNA-binding proteins with prion-like domains in neurodegenerative disease. *Brain Res.* **1462,** 61–80 CrossRef Medline
14. Buratti, E., Brindisi, A., Giombi, M., Tisminetzky, S., Ayala, Y. M., and Baralle, F. E. (2005) TDP-43 binds heterogeneous nuclear ribonucleoprotein A/B through its C-terminal tail: an important region for the inhibition of cystic fibrosis transmembrane conductance regulator exon 9 splicing. *J. Biol. Chem.* **280,** 37572–37584 CrossRef Medline
15. Ayala, Y. M., De Conti, L., Avendaño-Vázquez, S. E., Dhir, A., Romano, M., D'Ambrogio, A., Tollervey, J., Ule, J., Baralle, M., Buratti, E., and Baralle, F. E. (2011) TDP-43 regulates its mRNA levels through a negative feedback loop. *EMBO J.* **30,** 277–288 CrossRef Medline
16. Johnson, B. S., Snead, D., Lee, J. J., McCaffery, J. M., Shorter, J., and Gitler, A. D. (2009) TDP-43 is intrinsically aggregation-prone, and amyotrophic lateral sclerosis-linked mutations accelerate aggregation and increase toxicity. *J. Biol. Chem.* **284,** 20329–20339 CrossRef Medline
17. Igaz, L. M., Kwong, L. K., Chen-Plotkin, A., Winton, M. J., Unger, T. L., Xu, Y., Neumann, M., Trojanowski, J. Q., and Lee, V. M. (2009) Expression of TDP-43 C-terminal fragments *in vitro* recapitulates pathological features of TDP-43 proteinopathies. *J. Biol. Chem.* **284,** 8516–8524 CrossRef Medline
18. Zhang, Y. J., Xu, Y. F., Cook, C., Gendron, T. F., Roettges, P., Link, C. D., Lin, W. L., Tong, J., Castanedes-Casey, M., Ash, P., Gass, J., Rangachari, V., Buratti, E., Baralle, F., Golde, T. E *et al.* (2009) Aberrant cleavage of TDP-43 enhances aggregation and cellular toxicity. *Proc. Natl. Acad. Sci. U.S.A.* **106,** 7607–7612 CrossRef Medline
19. Michelitsch, M. D., and Weissman, J. S. (2000) A census of glutamine/asparagine-rich regions: implications for their conserved function and the prediction of novel prions. *Proc. Natl. Acad. Sci. U.S.A.* **97,** 11910–11915 CrossRef Medline
20. Lagier-Tourenne, C., and Cleveland, D. W. (2009) Rethinking ALS: the FUS about TDP-43. *Cell* **136,** 1001–1004 CrossRef Medline
21. Li, W., Reeb, A. N., Lin, B., Subramanian, P., Fey, E. E., Knoverek, C. R., French, R. L., Bigio, E. H., and Ayala, Y. M. (2017) Heat shock–induced phosphorylation of TAR DNA-binding protein 43 (TDP-43) by MAPK/ERK kinase regulates TDP-43 function. *J. Biol. Chem.* **292,** 5089–5100 CrossRef Medline

22. Kryndushkin, D. S., Alexandrov, I. M., Ter-Avanesyan, M. D., and Kushnirov, V. V. (2003) Yeast [PSI+] prion aggregates are formed by small Sup35 polymers fragmented by Hsp104. *J. Biol. Chem.* **278,** 49636–49643 CrossRef Medline
23. Bagriantsev, S. N., Kushnirov, V. V., and Liebman, S. W. (2006) Analysis of amyloid aggregates using agarose gel electrophoresis. *Methods Enzymol.* **412,** 33–48 CrossRef Medline
24. Halfmann, R., and Lindquist, S. (2008) Screening for amyloid aggregation by semi-denaturing detergent-agarose gel electrophoresis. *J. Vis. Exp.* **17,** 838 CrossRef Medline
25. Sanders, D. W., Kaufman, S. K., DeVos, S. L., Sharma, A. M., Mirbaha, H., Li, A., Barker, S. J., Foley, A. C., Thorpe, J. R., Serpell, L. C., Miller, T. M., Grinberg, L. T., Seeley, W. W., and Diamond, M. I. (2014) Distinct tau prion strains propagate in cells and mice and define different tauopathies. *Neuron* **82,** 1271–1288 CrossRef Medline
26. Bosque, P. J., Boyer, P. J., and Mishra, P. (2013) A 43-kDa TDP-43 species is present in aggregates associated with frontotemporal lobar degeneration. *PLoS One* **8,** e62301 CrossRef Medline
27. Guo, W., Chen, Y., Zhou, X., Kar, A., Ray, P., Chen, X., Rao, E. J., Yang, M., Ye, H., Zhu, L., Liu, J., Xu, M., Yang, Y., Wang, C., Zhang, D., *et al.* (2011) An ALS-associated mutation affecting TDP-43 enhances protein aggregation, fibril formation and neurotoxicity. *Nat. Struct. Mol. Biol.* **18,** 822–830 CrossRef Medline
28. Alberti, S., Halfmann, R., King, O., Kapila, A., and Lindquist, S. (2009) A systematic survey identifies prions and illuminates sequence features of prionogenic proteins. *Cell* **137,** 146–158 CrossRef Medline
29. Dewey, C. M., Cenik, B., Sephton, C. F., Johnson, B. A., Herz, J., and Yu, G. (2012) TDP-43 aggregation in neurodegeneration: are stress granules the key? *Brain Res.* **1462,** 16–25 CrossRef Medline
30. Udan-Johns, M., Bengoechea, R., Bell, S., Shao, J., Diamond, M. I., True, H. L., Weihl, C. C., and Baloh, R. H. (2014) Prion-like nuclear aggregation of TDP-43 during heat shock is regulated by HSP40/70 chaperones. *Hum. Mol. Genet.* **23,** 157–170 CrossRef Medline
31. Chen, H. J., Mitchell, J. C., Novoselov, S., Miller, J., Nishimura, A. L., Scotter, E. L., Vance, C. A., Cheetham, M. E., and Shaw, C. E. (2016) The heat shock response plays an important role in TDP-43 clearance: evidence for dysfunction in amyotrophic lateral sclerosis. *Brain* **139,** 1417–1432 CrossRef Medline
32. Vogler, T. O., Wheeler, J. R., Nguyen, E. D., Hughes, M. P., Britson, K. A., Lester, E., Rao, B., Betta, N. D., Whitney, O. N., Ewachiw, T. E., Gomes, E., Shorter, J., Lloyd, T. E., Eisenberg, D. S., Taylor, J. P., *et al.* (2018) TDP-43 and RNA form amyloid-like myo-granules in regenerating muscle. *Nature* **563,** 508–513 CrossRef Medline
33. Sampathu, D. M., Neumann, M., Kwong, L. K., Chou, T. T., Micsenyi, M., Truax, A., Bruce, J., Grossman, M., Trojanowski, J. Q., and Lee, V. M. (2006) Pathological heterogeneity of frontotemporal lobar degeneration with ubiquitin-positive inclusions delineated by ubiquitin immunohistochemistry and novel monoclonal antibodies. *Am. J. Pathol.* **169,** 1343–1352 CrossRef Medline
34. Bigio, E. H., Wu, J. Y., Deng, H. X., Bit-Ivan, E. N., Mao, Q., Ganti, R., Peterson, M., Siddique, N., Geula, C., Siddique, T., and Mesulam, M. (2013) Inclusions in frontotemporal lobar degeneration with TDP-43 proteinopathy (FTLD-TDP) and amyotrophic lateral sclerosis (ALS), but not FTLD with FUS proteinopathy (FTLD-FUS), have properties of amyloid. *Acta Neuropathol.* **125,** 463–465 CrossRef Medline
35. Neumann, M., Kwong, L. K., Sampathu, D. M., Trojanowski, J. Q., and Lee, V. M. (2007) TDP-43 proteinopathy in frontotemporal lobar degeneration and amyotrophic lateral sclerosis: protein misfolding diseases without amyloidosis. *Arch. Neurol* **64,** 1388–1394 CrossRef Medline
36. Robinson, J. L., Geser, F., Stieber, A., Umoh, M., Kwong, L. K., Van Deerlin, V. M., Lee, V. M., and Trojanowski, J. Q. (2013) TDP-43 skeins show properties of amyloid in a subset of ALS cases. *Acta Neuropathol.* **125,** 121–131 CrossRef Medline
37. Fang, Y. S., Tsai, K. J., Chang, Y. J., Kao, P., Woods, R., Kuo, P. H., Wu, C. C., Liao, J. Y., Chou, S. C., Lin, V., Jin, L. W., Yuan, H. S., Cheng, I. H., Tu, P. H., and Chen, Y. R. (2014) Full-length TDP-43 forms toxic amyloid oligomers that are present in frontotemporal lobar dementia-TDP patients. *Nat. Commun.* **5,** 4824 CrossRef Medline
38. Dhavale, D. D., Tsai, C., Bagchi, D. P., Engel, L. A., Sarezky, J., and Kotzbauer, P. T. (2017) A sensitive assay reveals structural requirements for alpha-synuclein fibril growth. *J. Biol. Chem.* **292,** 9034–9050 CrossRef Medline
39. Jiang, L. L., Che, M. X., Zhao, J., Zhou, C. J., Xie, M. Y., Li, H. Y., He, J. H., and Hu, H. Y. (2013) Structural transformation of the amyloidogenic core region of TDP-43 protein initiates its aggregation and cytoplasmic inclusion. *J. Biol. Chem.* **288,** 19614–19624 CrossRef Medline
40. Mompeán, M., Hervás, R., Xu, Y., Tran, T. H., Guarnaccia, C., Buratti, E., Baralle, F., Tong, L., Carrión-Vázquez, M., McDermott, A. E., and Laurents, D. V. (2015) Structural evidence of amyloid fibril formation in the putative aggregation domain of TDP-43. *J. Phys. Chem. Lett.* **6,** 2608–2615 CrossRef Medline
41. Shimonaka, S., Nonaka, T., Suzuki, G., Hisanaga, S., and Hasegawa, M. (2016) Templated aggregation of TAR DNA-binding protein of 43 kDa (TDP-43) by seeding with TDP-43 peptide fibrils. *J. Biol. Chem.* **291,** 8896–8907 CrossRef Medline
42. Chen, A. K., Lin, R. Y., Hsieh, E. Z., Tu, P. H., Chen, R. P., Liao, T. Y., Chen, W., Wang, C. H., and Huang, J. J. (2010) Induction of amyloid fibrils by the C-terminal fragments of TDP-43 in amyotrophic lateral sclerosis. *J. Am. Chem. Soc.* **132,** 1186–1187 CrossRef Medline
43. Cohen, T. J., Hwang, A. W., Unger, T., Trojanowski, J. Q., and Lee, V. M. (2012) Redox signalling directly regulates TDP-43 via cysteine oxidation and disulphide cross-linking. *EMBO J.* **31,** 1241–1252 CrossRef Medline
44. Taylor, J. P., Brown, R. H., Jr., and Cleveland, D. W. (2016) Decoding ALS: from genes to mechanism. *Nature* **539,** 197–206 CrossRef Medline
45. Mao, Y. S., Zhang, B., and Spector, D. L. (2011) Biogenesis and function of nuclear bodies. *Trends Genet.* **27,** 295–306 CrossRef Medline
46. Feric, M., Vaidya, N., Harmon, T. S., Mitrea, D. M., Zhu, L., Richardson, T. M., Kriwacki, R. W., Pappu, R. V., and Brangwynne, C. P. (2016) Coexisting liquid phases underlie nucleolar subcompartments. *Cell* **165,** 1686–1697 CrossRef Medline
47. Lin, Y., Protter, D. S., Rosen, M. K., and Parker, R. (2015) Formation and maturation of phase-separated liquid droplets by rNA-binding proteins. *Mol. Cell* **60,** 208–219 CrossRef Medline
48. Molliex, A., Temirov, J., Lee, J., Coughlin, M., Kanagaraj, A. P., Kim, H. J., Mittag, T., and Taylor, J. P. (2015) Phase separation by low complexity domains promotes stress granule assembly and drives pathological fibrillization. *Cell* **163,** 123–133 CrossRef Medline
49. Mackenzie, I. R., Nicholson, A. M., Sarkar, M., Messing, J., Purice, M. D., Pottier, C., Annu, K., Baker, M., Perkerson, R. B., Kurti, A., Matchett, B. J., Mittag, T., Temirov, J., Hsiung, G. R., Krieger, C., *et al.* (2017) TIA1 mutations in amyotrophic lateral sclerosis and frontotemporal dementia promote phase separation and alter stress granule dynamics. *Neuron* **95,** 808–816.e9 CrossRef Medline
50. Patel, A., Lee, H. O., Jawerth, L., Maharana, S., Jahnel, M., Hein, M. Y., Stoynov, S., Mahamid, J., Saha, S., Franzmann, T. M., Pozniakovski, A., Poser, I., Maghelli, N., Royer, L. A., Weigert, M., *et al.* (2015) A liquid-to-solid phase transition of the ALS protein FUS accelerated by disease mutation. *Cell* **162,** 1066–1077 CrossRef Medline
51. Tollervey, J. R., Curk, T., Rogelj, B., Briese, M., Cereda, M., Kayikci, M., König, J., Hortobágyi, T., Nishimura, A. L., Zupunski, V., Patani, R., Chandran, S., Rot, G., Zupan, B., Shaw, C. E., *et al.* (2011) Characterizing the RNA targets and position-dependent splicing regulation by TDP-43. *Nat. Neurosci.* **14,** 452–458 CrossRef Medline
52. Polymenidou, M., Lagier-Tourenne, C., Hutt, K. R., Huelga, S. C., Moran, J., Liang, T. Y., Ling, S. C., Sun, E., Wancewicz, E., Mazur, C., Kordasiewicz, H., Sedaghat, Y., Donohue, J. P., Shiue, L., Bennett, C. F., *et al.* (2011) Long pre-mRNA depletion and RNA missplicing contribute to neuronal vulnerability from loss of TDP-43. *Nat. Neurosci.* **14,** 459–468 CrossRef Medline
53. Lukavsky, P. J., Daujotyte, D., Tollervey, J. R., Ule, J., Stuani, C., Buratti, E., Baralle, F. E., Damberger, F. F., and Allain, F. H. (2013) Molecular basis of UG-rich RNA recognition by the human splicing factor TDP-43. *Nat. Struct. Mol. Biol.* **20,** 1443–1449 CrossRef Medline
54. Maharana, S., Wang, J., Papadopoulos, D. K., Richter, D., Pozniakovsky, A., Poser, I., Bickle, M., Rizk, S., Guillén-Boixet, J., Franzmann, T. M., Jahnel, M., Marrone, L., Chang, Y. T., Sterneckert, J., Tomancak, P., *et al.* (2018)

RNA buffers the phase separation behavior of prion-like RNA binding proteins. *Science* **360,** 918–921 CrossRef Medline

55. Guo, L., Kim, H. J., Wang, H., Monaghan, J., Freyermuth, F., Sung, J. C., O'Donovan, K., Fare, C. M., Diaz, Z., Singh, N., Zhang, Z. C., Coughlin, M., Sweeny, E. A., DeSantis, M. E., Jackrel, M. E., *et al.* (2018) Nuclear-import receptors reverse aberrant phase transitions of RNA-binding proteins with prion-like domains. *Cell* **173,** 677–692.e20 CrossRef Medline
56. Wegorzewska, I., Bell, S., Cairns, N. J., Miller, T. M., and Baloh, R. H. (2009) TDP-43 mutant transgenic mice develop features of ALS and frontotemporal lobar degeneration. *Proc. Natl. Acad. Sci. U.S.A.* **106,** 18809–18814 CrossRef Medline
57. Arnold, E. S., Ling, S. C., Huelga, S. C., Lagier-Tourenne, C., Polymenidou, M., Ditsworth, D., Kordasiewicz, H. B., McAlonis-Downes, M., Platoshyn, O., Parone, P. A., Da Cruz, S., Clutario, K. M., Swing, D., Tessarollo, L., Marsala, M., *et al.* (2013) ALS-linked TDP-43 mutations produce aberrant RNA splicing and adult-onset motor neuron disease without aggregation or loss of nuclear TDP-43. *Proc. Natl. Acad. Sci. U.S.A.* **110,** E736–E745 CrossRef Medline
58. Lim, L., Wei, Y., Lu, Y., and Song, J. (2016) ALS-causing mutations significantly perturb the self-assembly and interaction with nucleic acid of the intrinsically disordered prion-like domain of TDP-43. *PLoS Biol.* **14,** e1002338 CrossRef Medline
59. Conicella, A. E., Zerze, G. H., Mittal, J., and Fawzi, N. L. (2016) ALS mutations disrupt phase separation mediated by α-helical structure in the TDP-43 low-complexity C-terminal domain. *Structure* **24,** 1537–1549 CrossRef Medline
60. Gopal, P. P., Nirschl, J. J., Klinman, E., and Holzbaur, E. L. (2017) Amyotrophic lateral sclerosis-linked mutations increase the viscosity of liquid-like TDP-43 RNP granules in neurons. *Proc. Natl. Acad. Sci. U.S.A.* **114,** E2466–E2475 CrossRef Medline
61. Alami, N. H., Smith, R. B., Carrasco, M. A., Williams, L. A., Winborn, C. S., Han, S. S. W., Kiskinis, E., Winborn, B., Freibaum, B. D., Kanagaraj, A., Clare, A. J., Badders, N. M., Bilican, B., Chaum, E., Chandran, S., *et al.* (2014) Axonal transport of TDP-43 mRNA granules is impaired by ALS-causing mutations. *Neuron* **81,** 536–543 CrossRef Medline
62. Schmidt, H. B., and Rohatgi, R. (2016) *In vivo* formation of vacuolated multi-phase compartments lacking membranes. *Cell Rep.* **16,** 1228–1236 CrossRef Medline
63. Sanders, D. W., Kaufman, S. K., Holmes, B. B., and Diamond, M. I. (2016) Prions and protein assemblies that convey biological information in health and disease. *Neuron* **89,** 433–448 CrossRef Medline
64. Guo, J. L., and Lee, V. M. (2014) Cell-to-cell transmission of pathogenic proteins in neurodegenerative diseases. *Nat. Med.* **20,** 130–138 CrossRef Medline
65. Hasegawa, M., Arai, T., Nonaka, T., Kametani, F., Yoshida, M., Hashizume, Y., Beach, T. G., Buratti, E., Baralle, F., Morita, M., Nakano, I., Oda, T., Tsuchiya, K., and Akiyama, H. (2008) phosphorylated TDP-43 in frontotemporal lobar degeneration and amyotrophic lateral sclerosis. *Ann. Neurol.* **64,** 60–70 CrossRef Medline
66. Neumann, M., Kwong, L. K., Lee, E. B., Kremmer, E., Flatley, A., Xu, Y., Forman, M. S., Troost, D., Kretzschmar, H. A., Trojanowski, J. Q., and Lee, V. M. (2009) Phosphorylation of S409/410 of TDP-43 is a consistent feature in all sporadic and familial forms of TDP-43 proteinopathies. *Acta Neuropathol.* **117,** 137–149 CrossRef Medline
67. Furukawa, Y., Kaneko, K., Watanabe, S., Yamanaka, K., and Nukina, N. (2011) A seeding reaction recapitulates intracellular formation of sarkosyl-insoluble transactivation response element (TAR) DNA-binding protein-43 inclusions. *J. Biol. Chem.* **286,** 18664–18672 CrossRef Medline
68. Winton, M. J., Igaz, L. M., Wong, M. M., Kwong, L. K., Trojanowski, J. Q., and Lee, V. M. (2008) Disturbance of nuclear and cytoplasmic TAR DNA-binding protein (TDP-43) induces disease-like redistribution, sequestration, and aggregate formation. *J. Biol. Chem.* **283,** 13302–13309 CrossRef Medline
69. Scotter, E. L., Vance, C., Nishimura, A. L., Lee, Y. B., Chen, H. J., Urwin, H., Sardone, V., Mitchell, J. C., Rogelj, B., Rubinsztein, D. C., and Shaw, C. E. (2014) Differential roles of the ubiquitin proteasome system and autophagy in the clearance of soluble and aggregated TDP-43 species. *J. Cell Sci.* **127,** 1263–1278 CrossRef Medline
70. Walker, A. K., Spiller, K. J., Ge, G., Zheng, A., Xu, Y., Zhou, M., Tripathy, K., Kwong, L. K., Trojanowski, J. Q., and Lee, V. M. (2015) Functional recovery in new mouse models of ALS/FTLD after clearance of pathological cytoplasmic TDP-43. *Acta Neuropathol.* **130,** 643–660 CrossRef Medline
71. Porta, S., Xu, Y., Restrepo, C. R., Kwong, L. K., Zhang, B., Brown, H. J., Lee, E. B., Trojanowski, J. Q., and Lee, V. M. (2018) Patient-derived frontotemporal lobar degeneration brain extracts induce formation and spreading of TDP-43 pathology *in vivo*. *Nat. Commun.* **9,** 4220 CrossRef Medline
72. Wobst, H. J., Sharma, A., Diamond, M. I., Wanker, E. E., and Bieschke, J. (2015) The green tea polyphenol (−)-epigallocatechin gallate prevents the aggregation of Tau protein into toxic oligomers at substoichiometric ratios. *FEBS Lett.* **589,** 77–83 CrossRef Medline
73. Kedia, N., Almisry, M., and Bieschke, J. (2017) Glucose directs amyloid-β into membrane-active oligomers. *Phys. Chem. Chem. Phys.* **19,** 18036–18046 CrossRef Medline
74. Conway, K. A., Harper, J. D., and Lansbury, P. T. (1998) Accelerated *in vitro* fibril formation by a mutant α-synuclein linked to early-onset Parkinson disease. *Nat. Med.* **4,** 1318–1320 CrossRef Medline
75. Lesné, S., Koh, M. T., Kotilinek, L., Kayed, R., Glabe, C. G., Yang, A., Gallagher, M., and Ashe, K. H. (2006) A specific amyloid-β protein assembly in the brain impairs memory. *Nature* **440,** 352–357 CrossRef Medline
76. Sánchez, I., Mahlke, C., and Yuan, J. (2003) Pivotal role of oligomerization in expanded polyglutamine neurodegenerative disorders. *Nature* **421,** 373–379 CrossRef Medline
77. Klyubin, I., Walsh, D. M., Lemere, C. A., Cullen, W. K., Shankar, G. M., Betts, V., Spooner, E. T., Jiang, L., Anwyl, R., Selkoe, D. J., and Rowan, M. J. (2005) Amyloid β protein immunotherapy neutralizes Aβ oligomers that disrupt synaptic plasticity *in vivo*. *Nat. Med.* **11,** 556–561 CrossRef Medline
78. Ohhashi, Y., Ito, K., Toyama, B. H., Weissman, J. S., and Tanaka, M. (2010) Differences in prion strain conformations result from non-native interactions in a nucleus. *Nat. Chem. Biol.* **6,** 225–230 CrossRef Medline
79. Franzmann, T. M., Jahnel, M., Pozniakovsky, A., Mahamid, J., Holehouse, A. S., Nuske, E., Richter, D., Baumeister, W., Grill, S. W., Pappu, R. V., Hyman, A. A., and Alberti, S. (2018) Phase separation of a yeast prion protein promotes cellular fitness. *Science* **359**
80. Dulle, J. E., Bouttenot, R. E., Underwood, L. A., and True, H. L. (2013) Soluble oligomers are sufficient for transmission of a yeast prion but do not confer phenotype. *J. Cell Biol.* **203,** 197–204 CrossRef Medline
81. Nonaka, T., Masuda-Suzukake, M., Arai, T., Hasegawa, Y., Akatsu, H., Obi, T., Yoshida, M., Murayama, S., Mann, D. M., Akiyama, H., and Hasegawa, M. (2013) Prion-like properties of pathological TDP-43 aggregates from diseased brains. *Cell Rep.* **4,** 124–134 CrossRef Medline
82. Wang, Y. T., Kuo, P. H., Chiang, C. H., Liang, J. R., Chen, Y. R., Wang, S., Shen, J. C., and Yuan, H. S. (2013) The truncated C-terminal RNA recognition motif of TDP-43 protein plays a key role in forming proteinaceous aggregates. *J. Biol. Chem.* **288,** 9049–9057 CrossRef Medline
83. Saini, A., and Chauhan, V. S. (2011) Delineation of the core aggregation sequences of TDP-43 C-terminal fragment. *Chembiochem* **12,** 2495–2501 CrossRef Medline
84. Saini, A., and Chauhan, V. S. (2014) Self-assembling properties of peptides derived from TDP-43 C-terminal fragment. *Langmuir* **30,** 3845–3856 CrossRef Medline
85. Guenther, E. L., Ge, P., Trinh, H., Sawaya, M. R., Cascio, D., Boyer, D. R., Gonen, T., Zhou, Z. H., and Eisenberg, D. S. (2018) Atomic-level evidence for packing and positional amyloid polymorphism by segment from TDP-43 RRM2. *Nat. Struct. Mol. Biol.* **25,** 311–319 CrossRef Medline
86. Tavella, D., Zitzewitz, J. A., and Massi, F. (2018) Characterization of TDP-43 RRM2 partially folded states and their significance to ALS pathogenesis. *Biophys. J.* **115,** 1673–1680 CrossRef Medline
87. Yunus, A. A., and Lima, C. D. (2009) Purification of SUMO conjugating enzymes and kinetic analysis of substrate conjugation. *Methods Mol. Biol.* **497,** 167–186 CrossRef Medline

Detection of TAR DNA-binding protein 43 (TDP-43) oligomers as initial intermediate species during aggregate formation

Rachel L. French, Zachary R. Grese, Himani Aligireddy, Dhruva D. Dhavale, Ashley N. Reeb, Niraja Kedia, Paul T. Kotzbauer, Jan Bieschke and Yuna M. Ayala

J. Biol. Chem. 2019, 294:6696-6709.
doi: 10.1074/jbc.RA118.005889 originally published online March 1, 2019